ФИЗИКА ЭЛЕМЕНТАРНЫХ ЧАСТИЦ И АТОМНОГО ЯДРА
2004. Т. 35. ВЫП. 6

УДК 535.21:[539.143.5+539.144.4]

TRENDS IN LASER SPECTROSCOPIC INVESTIGATIONS OF NUCLEAR STRUCTURE

Marinova K. P.

Joint Institute for Nuclear Research, Dubna

ФИЗИКА ЭЛЕМЕНТАРНЫХ ЧАСТИЦ И АТОМНОГО ЯДРА
2004. Т. 35. ВЫП. 6

УДК 535.21:[539.143.5+539.144.4]

TRENDS IN LASER SPECTROSCOPIC INVESTIGATIONS OF NUCLEAR STRUCTURE

Marinova K. P.

Joint Institute for Nuclear Research, Dubna

Laser-spectroscopic methods of studying nuclei have led to a great deal of systematic experimental information on nuclear properties. The results include nuclear ground and isomeric state spins, magnetic dipole and electric quadrupole moments, and the behaviour of mean square nuclear charge radii within isotopic strings. These data give important information about the single-particle and collective effects on the nuclear structure. This review is devoted to the new generation of experimental laser spectroscopic methods giving access to very weak beams of isotopes far from stability. Special attention is paid to until now poorly investigated regions. They are the following: the exotic proton and neutron-rich low-Z nuclei around the neutron shell closures $N = 8, 20$; the very interesting calcium region around proton shell closure $Z = 20$ and with $20 \leqslant N \leqslant 28$; the neutron-rich medium Z elements and the very high-Z transeinsteinium nuclei.

К настоящему времени существует обширная экспериментальная информация о свойствах ядер, полученная методами лазерной спектроскопии. Эта информация касается спинов, магнитных дипольных и электрических квадрупольных моментов ядер, а также изменений среднеквадратичного зарядового радиуса в длинных изотопических цепочках. Эти величины содержат важные сведения об одночастичных и коллективных эффектах в ядерной структуре. Данный обзор посвящен новому поколению экспериментальных лазерно-спектроскопических методов, дающих доступ к очень слабым пучкам ядер, далеких от линии стабильности. Особое внимание уделено мало исследованным до сих пор областям ядер. Специально обсуждаются: экзотические протонно- и нейтронно-избыточные легкие ядра в окрестности нейтронных замкнутых оболочек $N = 8, 20$; особо интересна область кальция вблизи протонной замкнутой оболочки $Z = 20$ и с числом нейтронов в диапазоне $20 \leqslant N \leqslant 28$; нейтронно-обогащенные ядра элементов со средними значениями Z и тяжелые элементы ($Z \geqslant 92$), в частности трансэйнштейновские.

INTRODUCTION

In early nuclear physics, the main source of information on ground-state properties of the nucleus was Optical Spectroscopy by using spectral lamps and interferometers. Later, radio frequency methods such as Atomic Beam Magnetic Resonance, Double Resonance Spectroscopy or Optical Pumping were introduced. By these methods the interaction of the nucleus with the electromagnetic field produced by the electrons surrounding the nucleus, or with an electromagnetic field applied externally, was investigated. All these techniques, based on hyperfine structure splitting or isotope shift measurements, yield model-independent

Table 1. **Relation between nuclear and atomic properties**

Nucleus:	**Electronic shell:**
I — spin	J — intrinsic quantum number
μ_I — magnetic dipole moment	W_J — energy of atomic level
Q_s — electric quadrupole moment	ν — optical transition frequency
$\langle r^2 \rangle$ — ms charge radius	
Nucleus-electronic shell interaction:	**Hyperfine splitting** **Isotope shift**

Hyperfine splitting (hfs):

$$|J - I| \leqslant F \leqslant |J + I| \text{ with } \Delta F = 0, \pm 1$$

$$\Delta W_F = A\frac{C}{2} + B\frac{3C(C+1) - 4I(I+1)J(J+1)}{8I(2I-1)J(2J-1)} \quad (1)$$

$$\text{where} \quad C = F(F+1) - I(I+1) - J(J+1) \quad (2)$$

$$A = \frac{\mu_{\bar{I}}\overline{H(0)}}{IJ} \text{ and } B = eQ_s\overline{\varphi(0)_{JJ}} \quad (3)$$

ΔW_F — experimentally measured quantity from hfs; $\overline{H(0)}, \overline{\varphi(0)_{JJ}}$ — theoretically calculated quantity depending only on electron shell; μ_I, Q_s — nuclear parameters determined from A and B hyperfine coupling factors

Isotope shift (IS):

$$\delta\nu^{A'A} = \nu^A - \nu^{A'} = \delta\nu_{\mathrm{FS}}^{A'A} + \delta\nu_{\mathrm{MS}}^{A'A} \quad (4)$$

$$\text{Field shift (FS): } \delta\nu_{\mathrm{FS}}^{A'A} \approx F(Z)\delta\langle r^2\rangle^{A'A} \quad (5)$$

$$\text{Mass shift (MS): } \delta\nu_{\mathrm{MS}}^{A'A} = MS\frac{A - A'}{AA'} \quad (6)$$

$\delta\nu^{A'A}$ — experimentally measured IS; MS — mass shift constant — theoretically calculated or empirically determined quantity depending on the electron shell properties; $F(Z)$ — relativistic electronic factor; $\delta\langle r^2\rangle^{A'A}$ — change in ms nuclear charge radii

information about the nucleus [1]. The relation among the atomic and nuclear properties is briefly illustrated in Table 1.

At present, it is almost exclusively laser spectroscopic techniques that are used. Due to the large cross section for absorption of optical photons ($\approx 10^{-10}$ cm^2) and the high available laser intensity with small bandwidth, experiments with a single atom became possible [2, 3]. Thus, the laser spectroscopy methods are very sensitive tools for nuclear structure investigations. They allow one to determine with a high accuracy important nuclear parameters (spin

I, magnetic dipole moment μ, electric quadrupole moment Q, changes in mean square charge radii of nuclei $\delta\langle r^2\rangle$) for long chains of stable and radioactive isotopes in ground and isomeric states. The phenomena observed in the systematics of these quantities include collective properties and deformation, nuclear shape coexistence and shell effects. The occupation of single particle levels and the valence nucleon wave functions are reflected in the spins and magnetic moments.

Therefore it is not surprising that the very precise laser spectroscopic data stimulated, for example, the development of the nuclear shell models. Certainly, there was and still is a significant impact of atomic physics on nuclear physics. Also the opposite holds true. Nuclear physics has a strong impact on other branches of science, especially on atomic physics. For example, long isotopic chains, extending far off stability, are accessible at radioactive ion beam facilities, on-line isotope separator (ISOL), or in-flight facilities. They enable measurements over a large range of mass numbers and in this way provide a stringent test of the theory of isotope shift consisting of a volume and a mass effect. Many aspects of atomic spectroscopy of unstable isotopes and the status of the field in 1989 have been reviewed by Otten [3], who summarized also the measured spins, moments and changes in nuclear radii up to mid-1988. Gangrsky [4] has interpreted the experimental charge radii in terms of quadrupole deformation parameters. The most recent evaluation of the experimental isotope shifts is given by Frieke et al. [5], and a table of all nuclear moments including those deduced from the hyperfine structures has been compiled in [6, 7]. The systematics of nuclear charge radii are presented by Aufmuth et al. [8] and by Nadjakov et al. [9] who consider also the isotonic variation by introducing a global treatment to include muonic and electronic scattering data. An updated account of the contributions of laser spectroscopy to the study of nuclear sizes and shapes is given by Billows et al. [10].

Figure 1 reflects the *status quo* of some years ago and provides an overview of the systematic work on long chains of isotopes that has been so far performed. The plot also includes some off-line work on longer chains of stable or long-lived isotopes, such as, e.g., the important series of Ca isotopes [11, 12], or the long-lived U [13] and Th isotopes [14]. As one can see, there are still large blank fields. To specify some of these, the following examples should be mentioned:

i) The low-Z elements ($Z \leqslant 18$) with neutron number between shell closures $N = 8$ and $N = 20$: a region where interesting «exotic» phenomena have to be expected. The study of exotic nuclei has been at the forefront of nuclear physics research during the last years. Among the numerous advances made, one may cite the discovery of anomalous density distributions such as neutron haloes and skins [15, 16], a prediction of a possible proton halo [17], the alteration of the well-known magic numbers near the neutron drip line [18] ($N = 6$ instead $N = 8$ for nuclei with $Z < 8$; $N = 14$ and $N = 16$ instead $N = 20$ respectively for nuclei with $Z = 7$–10 and $Z = 7, 8$ [19]) and the appearance of the so-called

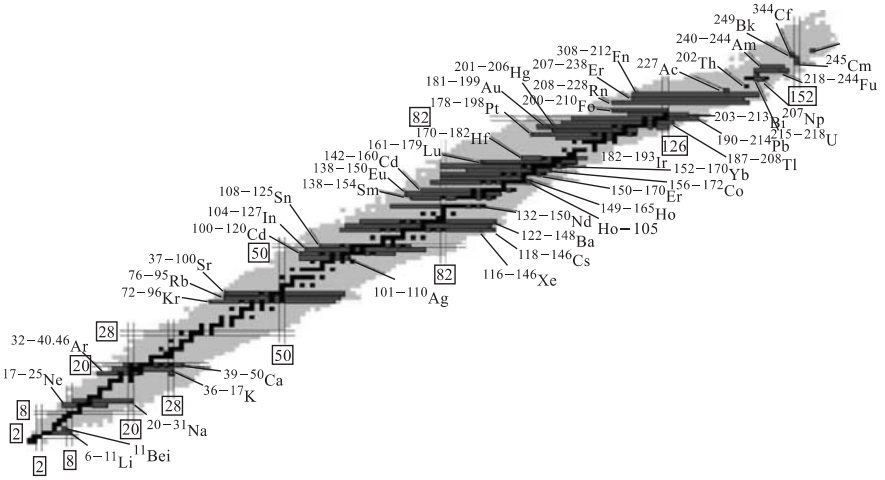

Fig. 1. Chart of nuclei showing the isotopes for which optical spectroscopy has been performed in long isotopic chains or on nuclei far from stability. Results cover the available experimental data till 1999 [28]

island of inversion. A striking example of the last phenomenon has already been observed at the shell closure $N = 20$ for the neutron-rich ^{31}Na [20, 21] and ^{32}Mg [22, 23] which, in spite of our conventional ideas, are strongly deformed.

ii) The very interesting calcium region around the proton shell closure $Z = 20$ and between the neutron magic numbers $N = 20$ and $N = 28$. It is presented with only two full isotopic sequences of K [24] and Ca [11, 12, 25], where an unusual behaviour of the charge radii has been observed. Results are also available in the case of the even-Z element titanium ($Z = 22$) for the stable $^{46–50}$Ti isotopes [26, 27] covering only the upper half of the $1f_{7/2}$ neutron shell. Altogether this data cannot form a sufficiently large basis for a systematic overview and interpretation of the development of the nuclear structure in the calcium region.

iii) The largest part of the elements between Ti and Kr as well as between Sr and Sn. From special nuclear interest are, first, the element around proton magic number $Z = 28$. The investigation of long isotopic sequences in this region will give new information on the isotonic nuclear radii behaviour and the proton shell closure effects which were considered already for the major proton magic numbers [3, 9]. Second, here we have the neutron rich isotopes of the above-mentioned elements, as well as of higher-Z elements with neutron numbers around neutron shell closures 50 and 82. The large neutron excess (in some cases 10–15 more neutrons than in the nuclei from the β-stability valley) could lead to an essential change in nuclear structure and radioactive decay characteristics.

The abnormal ratio of protons and neutrons in such nuclei reflects on spin-orbit interactions and can give rise to another order of filling the nucleon orbits. This will manifest itself as in the case (i) in an appearance of new magic numbers of protons or neutrons and new regions of deformation. Such situation could occur, e.g., for neutron-rich isotopes of Cu and Zn around $N = 50$ as well as in Ag and Cd isotopes around $N = 82$ [29].

iv) The region of very high-Z nuclei ($Z > 92$) remains still poorly investigated. Moreover, for the heavier transeinsteinium elements there are only *ab-initio* calculations on electron configurations but no experimental data are available. Appropriate laser technique would be necessary to measure atomic properties such as the first ionization potential or the atomic excitation schemes. When excited atomic states of the transeinsteinium elements are known the hyperfine structure of suitable transitions can also be studied. In this way, nuclear ground-state properties like spin, magnetic dipole and electric quadrupole moments and charge radii can be determined. Such data will enable a stringent test of the application of nuclear models to the heaviest nuclei.

In the last decade, new techniques for study of ground state properties of short-lived nuclides have been developed. Collinear laser spectroscopy invented and tailored for the determination of nuclear ground state properties of short-lived isotopes at ISOL-facilities [30, 31] and experimental method combining laser spectroscopy with β-NMR [32, 33] can be given as an example. It can be expected that the nuclear ground state properties will be determined for nearly all isotopes of the chart of nuclides that are produced with production yields exceeding about 100–1000 ions per second. In special cases, also dedicated laser experiments might be performed on nuclides available only in minute quantities of 1 ion/s or below. Thus, the planned or just realized radioactive ion beam facilities of the next generation will enable extension of our knowledge on nuclear ground state properties in isotopic chains to regions further from the valley of nuclear stability.

This review is devoted to the new generation of experimental methods and the main interest is moved from a systematic exploration of larger regions of the chart of nuclides to the poorly investigated «blank fields». We do not aim to give a complete discussion of all the spins, moments and nuclear radii that have been measured off stability in recent years. We wish to focus, on the one hand, on the new high sensitivity and high accuracy experimental methods and, on the other hand, on the most important experimental results belonging to the four regions mentioned above. Section 1 is devoted to the new experimental techniques developed at the ISOLDE-facility [30, 34] and to some results concerning the properties of light nuclei in the $1p$ and $2s1d$ shells, around the neutron shell closures $N = 8, 20$. In Sec. 2 we give a brief description of the IGISOL experimental technique [31]. Special attention is paid to the systematics of charge radii in the calcium region. In Sec. 3 the recent results on the long

isotopic sequence of Zr and the neutron rich Sn isotopes are used to illustrate the extension of our knowledge of nuclear ground state properties to regions further from the valley of nuclear stability. The extreme sensitive laser technique proposed in the SHIPTRAP-project (GSI, Darmstadt) for investigation of very high-Z (transeinsteinium) nuclei is considered in Sec. 4.

1. LOW-Z ELEMENTS AND EXOTIC NUCLEI

As pointed out in the Introduction, until now there exists a large lack of laser spectroscopic data for light nuclei ($Z \leqslant 18$), especially for the light exotic nuclei at the neutron or proton drip-lines, which were extensively discussed in the last years, see, e.g., the review papers [35, 36]. Such a situation is due to some reasons. The most fundamental problem is that the field shift contribution to the isotope shift becomes smaller while the mass shift becomes larger for lighter elements (Eq. (6) in Table 1), necessitating very small experimental errors on large optical frequency shift. For evaluating differences of mean square (ms) radii one has to know the mass shift very precisely. Also the atomic hyperfine fields decrease rapidly with Z [37], and as the nuclear quadrupole moments decrease as well, the quadrupole interaction of the hyperfine structure cannot easily be resolved for $Z \leqslant 20$. The problem of ultimate resolution adds to the standard problem faced by experiments on short-lived isotopes that the sensitivity of the method should be sufficiently high to deal with the small amount of nuclei produced by nuclear reaction at accelerator facilities. A variety of laser spectroscopic techniques have been developed for this purpose and it turns out that in particular for light elements these have to be tailored individually for the specific atomic level schemes and nuclear decay properties.

Laser spectroscopy of light elements was the general field of interest of the Collaboration COLLAPS — COLlinear LAser SPectroscopy at ISOLDE (CERN). An experimental programme based on the method of collinear laser spectroscopy was introduced at ISOLDE about 20 years ago. Experiments have been performed on a large amount of nuclides with the production rate exceeding 10^4–10^7 particles/s. Over the years many new ideas have been injected leading to an improvement of the experimental technique towards better resolution and sensitivity. Three advanced variants of collinear laser spectroscopy have been proven very successful in enhancement of the sensitivity: (i) State-selective collisional ionization of neutral beams and (ii) state-selective neutralization of ion beams both in combination with optical pumping and nonoptical detection [38–40]. (iii) In-flight polarization of the beams combining laser spectroscopy and β-NMR. The problem of resolution was tackled by the development of a method for high accuracy determination of the beam kinetic energy [41, 42] which ensures high accuracy in determination of the IS and hfs.

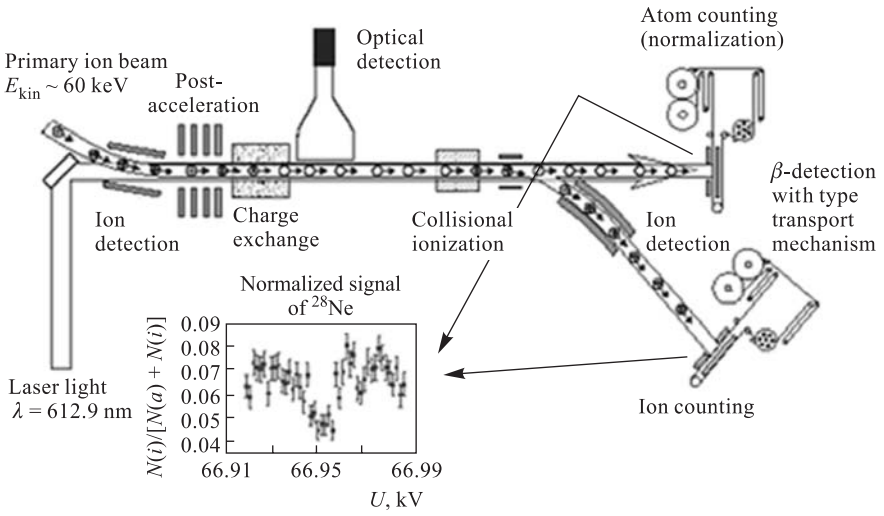

Fig. 2. Scheme of the experimental setup using collisional ionization and β-ray detection. A resonance signal of ^{28}Ne is shown in the inset. The spectrum was obtained using summation of the individual scans (each of duration of about 1.5 min) during 4.5 h [45]

1.1. Experimental Methods. ***1.1.1. Ultra Sensitive Laser Spectroscopy with State Selective Ionization (Atomization).*** The experimental setup at ISOLDE mass-separator at the CERN PS-Booster in its present view is shown schematically in Fig. 2. The mass-separated ion beam is superimposed collinearly on a cw laser beam. For the application of the state-selective reionization method, the primary mass-separated ion beam has firstly to be neutralized. The neutralization occurs in a charge-exchange cell containing alkali vapour neutralizing the beam in flight. Figure 3 illustrates, on the example of charge exchange between sodium atoms and neon ion beam, how a near resonant charge-exchange process can populate high lying metastable states [43]. A sodium vapour pressure of the order of 10^{-2} mbar, at temperature of about 550 K, was sufficient to achieve charge exchange rates up to 95% [44]. Atoms in this state can be excited resonantly by laser light to the $2p^5 3p[3/2]_2$ state which decays either back to $2p^5 3s[3/2]_2$ or cascades with high probability via intermediate $2p^5 3s[1/2, 3/2]_1$ state to the $2p^6$ $^1S_0$ ground state, as is shown in Fig. 3.

An electronic variation of the beam energy by a computer-controlled electrical potential applied to the charge-exchange cell is used to tune the optical frequency in the rest frame of atoms. The optical resonance signal can be detected by counting the fluorescence photons from the decay of the excited state. A drawback of the optical detection scheme is the low counting efficiency for fluorescence

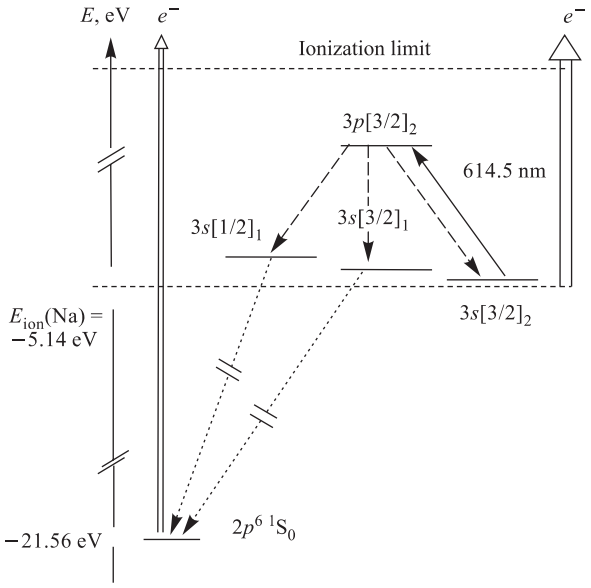

Fig. 3. Partial atomic level scheme of neon [46], optical pumping cycle and ionization energy of the charge exchange medium sodium

photons of about 10^{-4}, arising from the solid angle of the collection optics and the quantum efficiency of the photomultiplier. Moreover, a constant background from stray laser light is inherent to this technique. For studies on neutral atoms, the decay of excited states populated in the charge exchange process provides an additional source of background. And at last, the optical pumping prevents the multiple excitation of atom, except for a few cases such as resonance lines of Ba I [47].

A nonoptical detection method, based on collisional, state selective ionization is used to discriminate between atoms leaving the optical excitation region in different atomic states [43]. At resonance, optical pumping occurs from the metastable state to the ground state. Due to the larger ionization cross section of the excited state this gives rise to a decrease in the ionization rate. For short-lived isotopes it is favourable to detect the radioactive decay which is insensitive to background from isobaric beam contamination. The nonoptical detection technique was improved to avoid the variations in the measured ion signal due to the significant intensity variations of the primary ion beam. These are due to different causes and can hamper seriously the acquisition of spectra as a function of time. The problem was overcome installing a detector system in

the forward direction, identical to the one in the deflected direction (see Fig. 2). Thus, the nonionized fraction of the beam was also recorded. Normalizing the ion signal to the total beam intensity, a signal, which is independent of beam intensity fluctuations, is achieved.

There are two main reasons for the enormous gain in sensitivity achieved using this technique instead of optical detection. (i) The counting efficiency for ions is nearly 100% while for photons it is below 1%. (ii) The constant background due to stray laser light is avoided. Nevertheless, its application is restricted to rather pure beams because the purification of the contaminated beams by specific neutralization and collisional ionization processes turns out to be rather poor. The isobaric contaminations are largely suppressed by the cold transfer line between the production target and the ion source.

As a result, an ultrahigh sensitivity was achieved, allowing registration of even–even isotopes with half-lives smaller than hundred ms and yields from the separator of about 45 ions per ISOLDE pulse. This was achieved, e.g., in the case of ^{28}Ne ($T_{1/2} = 17$ ms) (see Fig. 2). In the cases of short-lived odd isotopes, hyperfine structure measurements were performed with yields from ISOLDE of about 10^3 ions per proton pulse. The scheme using state selective reionization of an optically pumped neutral atom beam was applied on long isotopic chains of noble gases — $^{72-96}$Kr [48], $^{32-40,46}$Ar [30] and $^{17-26,28}$Ne [44].

A similar idea was realized in a reversed sense on alkaline-earth ions. This consists of ground state depopulation by optical pumping via $ns\ ^2\mathrm{S}_{1/2} \rightarrow np\ ^2\mathrm{P}_{1/2,3/2}$ and spontaneous decay to $(n-1)d\ ^2\mathrm{D}_{3/2,5/2}$ metastable states [40]. The pumping effect was monitored by the state-selective neutralization on alkali vapour and charge state separated atom/ion counting.

1.1.2. β-NMR Spectroscopy. For measurements of nuclear moments there is an interesting alternative to atomic hyperfine structure studies. It is a combination of collinear fast-beam laser spectroscopy and RADOP, i.e., the Radio-Active Detection of Optical Pumping, via the β-decay asymmetry of polarized nuclei implanted into a catcher crystal. The first experiment was performed on-line with the ISOLDE facility at CERN [32, 33] using a mass separated lithium beam from proton fragmentation in a Ta-foil target (a typical yield of $2{\cdot}10^3$ ions/s). This beam is guided to the apparatus shown in Fig. 4. A quarter-wave plate in front of the entrance window converts the linear polarization of the laser light into circular, and the quantization axis for σ^+ and σ^- resonance absorption is established by a small ($B_\parallel \approx 4$ G) longitudinal magnetic field. The 60 keV lithium beam, neutralized by charge exchange with sodium vapour, is polarized by the transfer of angular momentum from the $\sigma^+(\sigma^-)$ polarized photons in the absorption process which is governed by the selection rule $\Delta m = +1(-1)$. Owing to the hyperfine interaction this atomic polarization also involves the nuclear spin. Downstream of the optical pumping zone the spins are rotated adiabatically into the direction of a strong transversal magnetic field $B_\perp \approx 5$ kG. The atoms are implanted into a

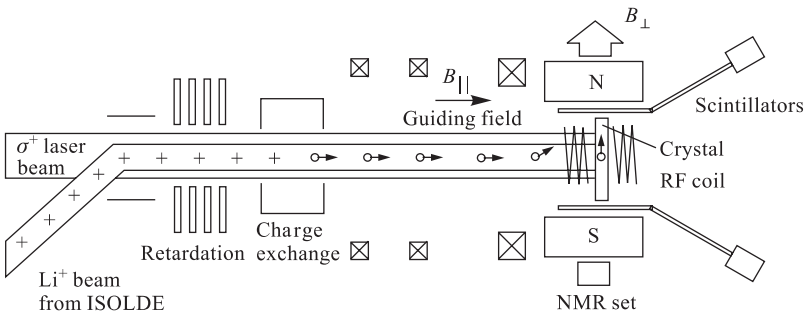

Fig. 4. Schematic view of the experimental setup used for in-beam optical polarization and β-NMR experiments

single crystal placed in the centre of this magnet and mounted with its symmetry axis parallel to $B_\perp$. During the implantation process the static magnetic field $B_\perp$ decouples the nuclear spin and the spin of the valence electrons. The β decay of the polarized nuclei is detected by two scintillation counter telescopes placed between the thin windows of the vacuum chamber and the magnet pole faces, parallel and antiparallel to $B_\perp$. The asymmetry is then defined as the normalized difference between the count rates of both telescopes,

$$a = \frac{N(0^\circ) - N(180^\circ)}{N(0^\circ) + N(180^\circ)}. \tag{7}$$

The experiments on ^{11}Li were performed in three steps using the same basic setup [34]. First, the β-asymmetry signal was used as a detector for optical resonance while the laser frequency was swept over the hyperfine structure of the lithium D_1-line. This essentially gave the ground state hyperfine structure. Then the laser frequency was fixed to the maximum asymmetry signal and a magnetic rf field perpendicular to $B_\perp$ at the position of the crystal was generated. The radiofrequency induces transitions between the magnetic sublevels m_I of the nuclear spin I. At the Larmor frequency the population is equalized and the asymmetry disappears. The results of these first two steps have been combined to yield the spin I and the magnetic moment μ_I of ^{11}Li.

While the measurements of the magnetic moment and the spin were performed in a crystal of cubic symmetry (LiF), the quadrupole interaction between the implanted nucleus and the internal electric field gradient of the lattice can be measured in a noncubic crystal, e.g., $LiNbO_3$. This interaction causes an equidistant splitting, Δ_Q, of the NMR signal into $2I$ components (see Fig. 5). Since Δ_Q is proportional to the quadrupole moment Q, a measurement of Δ_Q for two isotopes yields the ratio of their quadrupole moments. For isotopes with

low production rate, such as ^{11}Li, the technique is modified to enhance the signal intensity. The nuclear polarization was increased by an optimization of the magnetic field configuration, and an enhancement of the NMR signal was achieved by simultaneous application of all transition frequencies which only depend on the unknown quadrupole interaction once the Larmor frequency is known [34].

1.1.3. Determination of the Beam Kinetic Energy. In collinear laser spectroscopy the laser frequency ν_L is kept constant. Fine-tuning of the optical frequency in the ions frame only requires a change of the ion beam velocity. This is easily achieved by keeping the interaction region at a variable electrical potential (Fig. 2). Hence, the position of an atomic resonance is determined by the total kinetic energy of the atoms at resonance with the optical transition. The shifted transition frequency is connected to the beam energy in eV via the well-known Doppler shift formula where the «+» sign refers to a collinear superposition of the laser beam and the ion beam and the «−» sign to an anticollinear superposition of both beams:

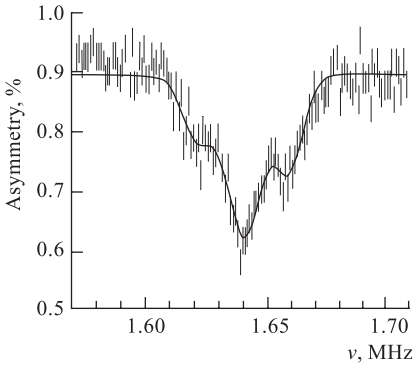

Fig. 5. β-NMR signal of ^{9}Li ($I = 3/2$) in $LiNbO_3$ using conventional single frequency scanning technique. Quadrupole splitting $\Delta_Q = 18.6(1.4)$ kHz [33]

$$\nu(\beta) = \nu_L = \nu_0 \frac{1 \pm \beta}{\sqrt{1-\beta^2}} \quad \text{with} \quad \beta = \frac{v}{c} = \frac{\sqrt{eU(2mc^2 + eU)}}{mc^2 + eU}. \tag{8}$$

Here ν_0 is the resonance frequency of the atomic transition in the rest frame of atoms. The relative beam velocity β is described with the relativistically correct formula depending on the beam energy eU and isotope mass m. According to Eq. (8), the Doppler shift between two neighbouring isotopes of light elements at beam energy of the order of 60 keV varies between 100 and 10 GHz in the mass region from $A \approx 8$ to $A \approx 40$. The expected volume effect is of the order of 10 MHz or even essentially smaller at the lower A limit. In average, one has to measure an effect of the order of 10^{-4}. This requires accuracy in determination of the peak position better than 10^{-5}, which at 60 kV acceleration potential is about 0.6 V. Such precision is not supplied by the standard measurement methods [47].

To measure the kinetic beam energy of the incoming ion beam from the mass separator with sufficient accuracy, a method which can be performed by using an ion beam of stable neon isotopes was developed [42]. The method is a modification of technique for measuring the ion beam energy proposed by

Poulsen [49]. It is based on the fact that two optical transitions, separated by twice the Doppler shift can be excited at the same laser frequency in collinear and anticollinear laser beam — atomic beam geometry. Since the atomic transitions are excited at the one laser frequency, they have to fulfil the condition

$$\begin{aligned} \nu_L &= \frac{\nu_0^+}{mc^2}\left[mc^2 + eU^+ + \sqrt{eU^+(2mc^2 + eU^+)}\right] \;-\; \text{collinear}, \\ &= \frac{\nu_0^-}{mc^2}\left[mc^2 + eU^- - \sqrt{eU^-(2mc^2 + eU^-)}\right] \;-\; \text{anticollinear}. \end{aligned} \tag{9}$$

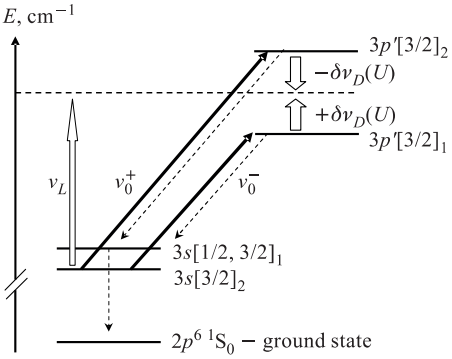

Fig. 6. Atomic levels of NeI participating in the collinear-anticollinear excitation for the voltage calibration. The thick full-line arrows indicate the excitation in the frame of moving atoms by laser-light at $\nu_L = 16773.41$ cm^{-1}. The dashed-line arrows indicate the radiative de-excitation in the moving frame of the atom. The hollow arrows indicate the Doppler shifts

The Doppler shifted frequencies match at a definite beam energy $eU_{\text{cross}} = eU^+ = eU^-$, which can be obtained from (9), and can be used to determine the energy of an ion beam at resonance with laser. The atomic spectrum of neon offers transitions suitable to calibrate beam energies of about 60 keV (Fig. 6). Two suitable transitions start from the common $2p^5 3s[3/2]_2$ metastable state populated in the charge transfer reaction. The wave numbers of both transitions are known from external sources with a high precision [50, 51] and thus, they serve as a secondary wavelength standards. By this method the average beam energy of about 60 keV can be measured with a precision ≈ 0.3 eV. This corresponds to a level of accuracy required for the determination of IS and hfs with systematic uncertainties, e.g., for $\Delta m = 6$, not exceeding 0.3 to 2 MHz (the lower limit applies to the $A = 40$ and upper to $A = 8$).

The method is very convenient and can be used for more general applications connected with the development of ISOL technique. On-line mass separators delivering mass separated low energy ion beams are available at many basic nuclear physics facilities all over the world allowing production of a wide range of nuclei with relatively high production yield, see, e.g., ISOLDE at CERN [52], IGISOL at Yuväskylä [53]. Exciting new techniques have been developed giving rise to numerous experiments ranging from solid-state, atomic to nuclear physics. Facilities as SHIP at GSI [54], and, e.g., a recoil separator in Argonne (USA), enable the rich variety of physics experiments currently performed at ISOL facilities to

be extended to isotopes for which target/ion source systems do not exist at ISOL facilities. The experimental study of many new phenomena demands a continuous growth in energy resolution and, therefore, the requirements to a detailed knowledge of the absolute energy of the accelerated ions are increasing. These requirements are met by the optical method described above.

1.2. Experimental Results and Discussion. ***1.2.1. Properties of Exotic Nuclei Measured by Laser and β-NMR Spectroscopy.*** In the bottom part of the chart of nuclides, the momentum and charge radii of the exotic (halo and proton drip) nuclei are of considerable current interest. Halo nuclei are weakly bound nuclear systems at the neutron or proton drip line, which have a neutron (proton) density that extends far beyond the core of the nucleus [34]. A number of such nuclei have been studied quite extensively, mainly using reactions induced by radioactive ion beams [36]. The first indication of the halo structure of neutron-rich light nuclei came from the measurements of interaction cross sections of radioactive fragment nuclei with different targets. For a few systems such as ^{6}He, ^{8}He, ^{11}Li, and ^{11}Be, these cross sections were found to be exceptionally large [15]. Correspondingly large rms matter radii were deduced from a Glauber-model analysis of the experimental data. Initially this was taken as an indication for either a large deformation or a long tail in the matter distribution of the nuclei. It was soon pointed out [55] that a one or two neutron halo with an extended wave function should develop as a natural consequence of the low binding energy of the last neutron or neutron pair. Halo structures are most clearly demonstrated in the narrow momentum distributions of either neutrons or the core in break-up reactions (see [35] and the references therein). Despite the marked influence of different reaction mechanisms [56], these features reflect the momentum distribution of the weekly bound nucleons which is related to the spatial density distribution by a Fourier transform.

Although the halo picture has been developed from observations on nuclear reactions, it describes a static property of the nuclear ground state. Static observables such as nuclear moments and charge radii from atomic spectroscopy are not directly sensitive to neutron distributions, because the shell electrons probe the nuclear charge. Still they provide important information on nuclear structure. On the other hand, proton halos should be directly reflected in the charge radii and, if $I > 1/2$, in the electrical quadrupole moments. Here we will give three illustrative examples for the role of atomic spectroscopy observables for the exploration of halo structures.

(i) Nuclear Moments of ^{11}Li. ^{8,9}Li and the two neutron halo ^{11}Li are the lightest short-lived nuclei for which the spin and the magnetic moment as well as the spectroscopic quadrupole moment were determined by laser spectroscopy. A pronounced two-neutron halo structure was first postulated to explain the unusual large matter radius of ^{11}Li. The alternative explanation — the appearance of a large deformation could be ruled out when the spin and the magnetic moment

were measured in an experiment combining laser spectroscopy and β-NMR (Subsec. 1.1.2). The results for ^{11}Li were [32]: $I = 3/2$ and $\mu_I = 3.6673\mu_N$, both supporting the assumption of a spherical structure. With a magnetic moment close to the Schmidt value, the unpaired proton should be in a rather pure (spherical) $\pi 1p_{3/2}$ state, whereas a deformed structure would be associated with the [110]1/2 Nilsson level. Later, with a refined β-NMR technique it became even possible to measure the nuclear quadrupole moment. The quadrupole moment of ^{11}Li is only slightly larger than the one of ^{9}Li: $|Q(^{11}\mathrm{Li})/Q(^{9}\mathrm{Li})| = 1.14(16)$. This result further supports the picture of a spatially extended cloud of two neutrons barely influencing the electromagnetic properties produced by the ^{9}Li core [33]. Thus, the laser and NMR spectroscopy measurement on ^{11}Li excluded a deformed structure. It is to expect that an improvement of the accuracy of the ^{11}Li quadrupole moment should clear more definitely the predicted two neutron halo picture.

Since the matter radius of ^{11}Li is known, a measurement of the charge radius by isotope shift determination would allow one to deduce that of the neutron distribution. Presently an experiment is prepared to measure the charge radii of ^{11}Li with respect to ^{9}Li [57]. The challenges are to achieve high detection efficiency for this short-lived isotopes ($T_{1/2} = 9$ ms), to measure the isotope shift, which is around 10 GHz for ^{11,9}Li, with an accuracy of about 100 kHz, and to extract the tiny volume effect by use of calculated mass shift [58, 59]. A promising approach to rich this accuracy is pursued at GSI, Darmstadt. The idea is to prepare a thermal atomic beam and to use Doppler free two-photon absorption for high resolution with a subsequent two-step photo-ionization process for the extremely sensitive detection [60].

(ii) Magnetic Moment of ^{11}Be. ^{11}Be is the best known case of a one-neutron halo nucleus, and it has been studied quite extensively, mainly using reactions induced by radioactive ion beams. While for ^{11}Li the nuclear moments are only indirectly related to the halo structure, the magnetic moment of ^{11}Be is directly produced by the single halo neutron.

^{11}Be has two bound states ($1/2^+$ and $1/2^-$), both presenting a halo structure, which are connected by a very strong $E1$ transition [61]. Contrary to what one would expect from the standard shell model, the ground state is not $p_{1/2}$ but a $1/2^+$ intruder state from the sd shell. Various theoretical approaches have been proposed trying to reproduce these peculiar properties. Concerning the structure of the lowered $1/2^+$ state nearly all models suggest that the main component of the wave function is $|(^{10}\mathrm{Be})0^+ \times \nu 2s_{1/2}\rangle$, whereas the predicted admixture of the core excited $|(^{10}\mathrm{Be})2^+ \times \nu 2d_{5/2}\rangle$ state ranges from 10 to 40%. The magnetic moment should be particularly sensitive to the relative amplitudes of these two components. Thus, in combination with a theoretical analysis, a measurement of the magnetic moment of ^{11}Be would give detailed information about the wave function of the halo nucleus.

Using β-NMR Geithner et al. [62] obtained the magnetic moment of ^{11}Be, $\mu(^{11}\mathrm{Be}) = -1.6816(8)\mu_N$. It should reflect the composition of the ^{11}Be ground-state wave function [34]

$$\mu = \alpha^2\mu(\nu s_{1/2}) + \frac{7}{2}\beta^2\mu(\nu d_{5/2}) - \frac{1}{3}\beta^2\mu(2^+). \tag{10}$$

Here α and β denote the amplitudes of $|(^{10}\mathrm{Be})0^+ \times \nu 2s_{1/2}\rangle$ and $|(^{10}\mathrm{Be})2^+ \times \nu 2d_{5/2}\rangle$, respectively. Susuki et al. [63] used empirical values of the individual magnetic moments entering into (10) and obtained predictions between $-1.45\mu_N$ and $-1.62\mu_N$ for $s_{1/2}$ contributions between 60 and 100%. Shell-model calculations in a large p-sd model space have been reported by several authors (see, e.g., [64, 65]) and their predictions are generally about $-1.5\mu_N$. Only an early calculation based on the Millener–Kurath effective interaction [66, 67], yielding $-1.71\mu_N$ with $\alpha^2 = 0.82$, gets rather close to the experimental value. The predicted values were calculated using free nucleon g factors.

For lack of sufficient empirical data it is not clear to what extend additional core polarization would require effective (quenched) g factor. On the other hand, core polarization by a halo neutron may be appreciably smaller than for a well-bound unpaired neutron. Apart from these details one may conclude that the $|\nu 2s_{1/2}\rangle$ component in the wave function is by far dominant. The shell-model calculations not accounting for the exotic spatial structure of the ^{11}Be wave function will implicitly overestimate the quenching of the g factor. Presumably, the shell-model prediction of about $-1.5\mu_N$ compared to the experimental value of $-1.68\mu_N$, is influenced by this effect [62].

Note, that similar information about the wave function of the ^{11}Be neutron halo state is obtained from spectroscopic factors of the $p(^{11}\mathrm{Be},^{10}\mathrm{Be})d$ transfer reaction [68] and from the one-neutron knockout observed from the individual single-particle states of ^{11}Be [69]. For a more quantitative interpretation of the magnetic moment, the theoretical approaches should more explicitly account for the halo properties.

(iii) Proton-Drip Nucleus ^{17}Ne. The optical isotope shift probes very sensitive small changes in the nuclear charge distribution. This should help to reveal the appearance of proton halo. The proton drip-line nucleus ^{17}Ne is of particular interest. With two valence protons bound by only 0.96 MeV and a relatively large matter radius [70], ^{17}Ne is seriously considered as a proton halo candidate [17, 70–72]. Whereas the halo structure is well established for light neutron rich nuclei, the occurrence of proton halos in nuclei at the proton drip line is still under discussion. In any case the halo structure is expected to be less pronounced for weakly bound protons than for neutrons because of the Coulomb barrier. Especially, the evidence for ^{17}Ne is not conclusive and further experimental and theoretical studies are needed to clarify the case.

Using β-NMR and titled foil polarization, Baby et al. [73] obtained $\mu(^{17}\mathrm{Ne}) = +0.74(3)\mu_N$. An essentially more precise value of the ^{17}Ne magnetic moment has been deduced by the COLLAPS collaboration using ultra sensitive and high resolution laser spectroscopy with state selective ionization: $\mu(^{17}\mathrm{Ne}) = +0.7879(6)\mu_N$. A qualitative analysis based on: (i) a comparison of the magnetic moments of ^{17}Ne [44] and its mirror partner ^{17}N [74] and (ii) the Sugimoto [75] systematics of the isoscalar moments of conjugated nuclei, provides two serious arguments for the conclusion that ^{17}Ne, in spite of its small two-proton separation energy, should not be considered as a halo nucleus.

Calculations of the ^{17}Ne moment have been performed in the cross-shell $0\hbar\omega$ model space connecting the $\nu 1p$ and $\pi 2s1d$ shell [73] using the WBP interaction from [76]. The predicted magnetic moment $\mu(^{17}\mathrm{Ne}) = 0.795\mu_N$ is larger than the experimental. The agreement with experiment could be made exact if the contribution from the two sd-shell protons is reduced. This might be related to an admixture of the $(\pi 2s_{1/2})$ «halo» state to the $(\pi 1d_{5/2})$ ground state. Such conclusion is in agreement with the calculations of the ground state wave function of ^{17}N [74] and ^{17}Ne [77] giving similar amplitudes of $(1d_{5/2})^2$ and $(2s_{1/2})^2$ for the neutrons in ^{17}N and the protons in ^{17}Ne. Let us note, that the simultaneous investigation of the proton and neutron density distribution and the corresponding radii of ^{17}Ne and ^{17}N by a three-cluster generator-coordinate method [78], indicates no halo properties for ^{17}Ne, although a high probability for the ^{17}Ne valence protons to occupy $(\pi 2s_{1/2})^2$ state is involved. Two additional facts contradict the assumption of a proton halo in ^{17}Ne: i) the value of $S_{2p}A^{2/3} = 6.3$ MeV (S_{2p} — two proton binding energy) is too large to satisfy a (necessary but not sufficient) criterion given by [16] for halo existence; ii) experimentally, indirect information about momentum distributions of weekly bound protons seems to argue against a halo [79].

1.2.2. Nuclear Moments and Charge Radii of sd-Shell Isotopes. *(i) Quadrupole Moments of Radioactive Sodium Isotopes.* The disappearance of a spherical $N = 20$ shell closure in neutron rich nuclei with proton numbers far below $Z = 20$ (see Introduction) has been predicted theoretically [80–82] and established from mass measurements [20] and from nuclear spectroscopy [22]. Isotope shift measurements on the sodium isotopes give an indication of increasing radii towards ^{31}Na [21]. Quadrupole moments from the hyperfine structure have been determined long ago for $^{25-29}$Na [83], but they have exceedingly large errors. Recently, the β-NMR spectroscopy in noncubic crystals was used [84, 85] to obtain improved values for the nuclear electric quadrupole moments of the neutron rich sodium isotopes $^{26-31}$Na up to $N = 20$ and of ^{20}Na at the proton drip line. Sign information on the quadrupole moment is contained in the relative intensities of the $2I$ equidistant resonances forming the complete NMR spectrum for a nucleus with spin I (for details see [84, 85]).

A compilation of the quadrupole moments in a long isotopic sequence of sodium isotopes is presented in Fig. 7. The quadrupole moments are compared to theoretical values obtained from large-basis shell model calculations based on empirical effective (USD) interaction and using established effective charges, $e_p = 1.35$ and $e_n = 0.35$ [86, 87]. Two theoretical values are shown for the isotopes close to $N = 20$: (a) including only configurations of the sd shell and (b) taking into account the intruder states from the fp shell. It is seen, that the fp admixture has little effect for ^{29}Na, but improves decisively the theoretical value for ^{30}Na [85]. The different sign of both theoretical values shows the importance of experimental sign information for the theoretical interpretation of the data. For ^{31}Na the rather different wave functions of both calculations happen to give nearly the same quadrupole moment.

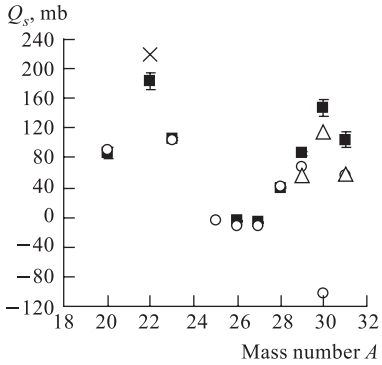

Fig. 7. Experimental quadrupole moments of sodium isotopes compared to theory. The full black squares denote experimental values: ^{22}Na [88], ^{23}Na [89, 90], $^{26-29}$Na [84], and ^{20,30,31}Na preliminary values [85]. The theoretical values represent pure sd shell calculations [84] (open circles), [87] (crux) and calculations including admixtures of fp intruder states (open triangles) (see [85])

The experimental value of the spectroscopic quadrupole moment of ^{31}Na ($I = 3/2$) is of the order of that of the stable ^{23}Na ($I = 3/2$) which is regarded as a well deformed nucleus. If one assumes that the well-known projection formula holds for ^{31}Na, one can conclude that both ^{23}Na and ^{31}Na have nearly the same intrinsic quadrupole moment. Confirming this will be a further experimental indication of deformed nuclear shape for neutron rich nuclei at the shell closure $N = 20$.

(ii) Nuclear Charge Radii in the Isotope Sequence $^{17-26,28}$Ne. For many years sodium has been the lightest element for which systematic information about ms nuclear charge radii of radioactive isotopes has been available [21, 83]. The problem of separating the small field shift and the large mass shift contributions was circumvented by a parameterization of the results, which leaves the extraction of absolute radii differences to additional assumptions from nuclear model. For neon, which has three stable isotopes, one can use experimental data [5] from muonic atom spectroscopy to overcome this problem. This means that the neon charge radii can be determined not only qualitatively but even quantitatively. Thus, nuclear shape in the sd shell can be revealed.

The charge radii of neon isotopes have been investigated by collinear fast-beam laser spectroscopy in combination with ultra-sensitive collisional ionization

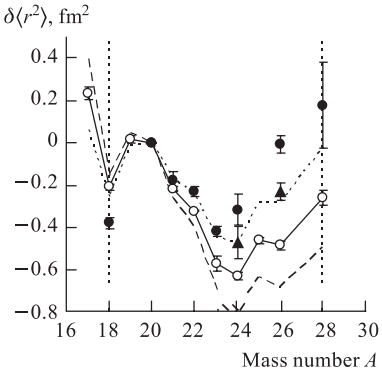

Fig. 8. A-dependence of $\delta\langle r^2\rangle$ for the Ne isotopes. Open circles — the experimental data [41, 44]. The error bars represent statistical errors; the systematic uncertainties arising from the calibration factors, $F(Z)$ and MS (see Table 1) are indicated by the two enveloping lines. The finite range droplet model values of $\delta\langle r^2\rangle_{\rm DM}$ [97] are denoted with full circles; both full triangles present data of $\delta\langle r^2\rangle_{\rm DM}$ obtained with negative β_2 value

detection and a method for high accuracy determination of the beam kinetic energy [41, 44]. The sequence of isotopes under study ranges from the proton-drip nucleus ^{17}Ne to the neutron-rich ^{26}Ne and ^{28}Ne. The ms charge radius goes through a minimum at the midshell and increases towards both neutron shell closures $N = 8$ and $N = 20$ (Fig. 8). The general trend of the charge radii can be explained qualitatively with competition of two effects: an increase of the proton binding energy with addition of neutrons leading to a decrease of the charge radius and a strong neutron-proton interaction at larger neutron excess pulling the protons outwards [91]. It is strongly distorted by the deformation effects which are very large for all Ne nuclei (see, e.g., [82, 92–95]) in the sd shell and originate charge radii variation very similar to the observed ones. In the scope of this picture, the case of ^{17}Ne must be treated with great care. The increase of the charge radius at the proton drip-line may be predominantly due to the first effect described above: the increase of the charge radius with decreasing the proton binding energy, which as already shown [96], does not exclude an influence of deformation effects, too. The nuclear charge radius of ^{17}Ne does not support a pronounced proton halo structure. As pointed out above, description which treats the nuclear structure of ^{17}Ne as dominated by a $d_{5/2}$ state with an $s_{1/2}$ admixture seems to be more likely.

In the last years a number of large theoretical papers have been published employing various models to investigate nuclear properties like masses, radii, and deformations all over the nuclear chart with different methods [93, 95, 98, 99]. For the Ne isotopic sequence the predicted variation of the nuclear charge radii shows peculiar behaviour: the light isotopes exhibit higher charge radii as compare to their heavier counterparts. The charge radii assume a minimum value nearly in the midshell and again increase for heavier masses. Thus, the general development of the experimental charge radii is described qualitatively well. But the theoretical curves lie well above the experimental. The HF calculations [95] seem to give the most realistic description of nuclear ground state properties in the region of

the even–even isotopes of O, Ne, and Mg. In contradiction to [95] the calculation of Goriely et al. [93] was intended for a large scale mass table. Nevertheless, it yields good agreement for the radii of the heavy, $A > 24$, and ^{18}Ne isotopes. It is the only calculation predicting a moderately nonspherical shape of ^{18}Ne. Thus, the magicity of $N = 8$ is not retained from experiment as well as from [93] calculations. The single particle influence of the two protons above the doubly magic ^{16}O configuration seems to be responsible for deformation. This assumption is strongly supported by the success of the droplet model description presented in Fig. 8. Its correlation with the experimental radii would obviously be better if one assumes a shape transition from prolate to oblate at the sd midshell, which is as well supported by all theoretical predictions [93, 98, 100, 101].

Due to a remarkable similarity between the trends of Ne and Na nuclear charge radii in the upper sd shell, the heavy Ne isotopes (in the vicinity of $N = 20$) seem to belong to the so-called «island of inversion». The latter is supposed to be produced by the influence of the fp intruder states [91]. Recent experimental and theoretical study [82] of the spectroscopy of the low lying states in the neutron rich isotopes ^{26,28}Ne suggest that both nuclei are located in the island of inversion or on its periphery. The results provide a complete picture of the role of deformed intruder configurations outside the boundaries of the island of inversion.

(iii) Nuclear Properties of Argon Isotopes in sd Shell by Laser Spectroscopy. The hfs and IS measurements on $^{32-40}$Ar and ^{46}Ar are the first optical high resolution investigations of argon [30]. The study of isotopes far from stability has become possible due to the ultra-sensitive resonance detection technique combining optical pumping and state selective collisional ionization with an isotope selective detection of ions based on the β decay (Subsec. 1.1.1). The results comprise magnetic dipole and electric quadrupole moments of the odd-A isotopes (Table 2) which were employed as a test of shell-model calculations for the sd and fp shells. Even far from stability a very good agreement between the experiment and theory [102] is found for these quantities. Thus, the electromagnetic moments prove the good predicative power of the sd shell calculation of Brown and Wildenthal [102] with the W interaction for short lived nuclei in the upper

Table 2. **Experimental and calculated magnetic dipole and electric quadrupole moments of argon nuclei in the sd shell and of ^{39}Ar with mixed sd-fp configuration according to [30]**

	I	μ^{exp}/μ_N	μ^{th}/μ_N	Q^{exp}, mb	Q^{th}, mb
^{33}Ar	1/2	$-0.723(6)$	-0.739		
^{35}Ar	3/2	0.633(2)	0.688	$-84(7)$ [8]	-88.7
^{37}Ar	3/2	1.145(5)	1.155	76.2(1.6) [7, 6]	76.1
^{39}Ar	7/2	$-1.588(15)$	-1.436	$-117(20)$ [12]	-128

sd shell. The results are from considerable interest especially in the case of the quadrupole moments, Q_s, since information about Q_s of unstable sd-shell nuclei is rather scarce.

Also, the changes in ms charge radii of Ar isotopes between $N = 14$ and $N = 22$, and at $N = 28$ have been measured. These results, together with the recent data on argon isotopes $^{40-44}$Ar [41, 104], cover the upper part of the sd shell and nearly the whole $\nu f_{7/2}$ shell. They will be discussed in Subsecs. 2.2 and 2.3.

1.3. Summary. Six prominent examples are chosen to demonstrate the unique possibilities of ISOLDE for high-resolution laser and β-NMR spectroscopy. During the past decade the experiments were focused on light nuclear systems, where they contributed important pieces of information to nuclear structure research.

• Experiments on ^{11}Li clearly demonstrate, from the spin, the magnetic moment and the electric quadrupole moment data, that the unusual spatial structure is not related to deformation effects.

• For ^{11}Be the magnetic moment produced by the halo neutron confirms the assumption of an $s_{1/2}$ wave function with a relatively small admixture of core-excited states.

• The IS and the magnetic moment of ^{17}Ne are not in favour of a proton halo.

• High-accuracy measurements of the quadrupole moments in a long isotopic sequence of sodium ($^{26-29}$Na) have been performed providing a good qualitative test of the theory. An increasing nuclear deformation toward the neutron magic number $N = 20$ has been indicated. The measurements could be extended to the neutron shell closure $N = 20$ and beyond, provided the beam intensities of these nuclei can be increased.

• Data on the isotope shift in an extended chain of neon isotopes ranging from the proton drip nucleus ^{17}Ne to the neutron rich ^{26}Ne and ^{28}Ne has been obtained reflecting the development of the nuclear ms charge radii for the lowest-Z isotope chain ever studied.

• Nuclear moments and charge radii of long isotopic sequence of argon isotopes ($^{33-44,46}$Ar) have been investigated providing new information to the systematics of radii in the Ca region (see Sec. 2).

Measurements of nuclear moments of magnesium isotopes, in particular those near the shell closures $N = 8$ and $N = 20$, have been proposed [105]. With the ISOLDE RILIS (Resonant Ionization Laser Ion Sources) clean beams of Mg isotopes have become available for experiments on the nuclear structure all the way through the sd shell. The ground state magnetic dipole and electric quadrupole moments of short-lived isotopes should be well accessible to the techniques of β-NMR spectroscopy. From the nuclear physics point of view there is a special interest in both regions that are accessible to this technique. ^{21}Mg at the proton drip line, for which the spin is not known, has one neutron

outside the closed $N = 8$ shell and continue the sequence of isotones ^{17}O, ^{19}Ne for which the ground state properties are well known. For the systematics of mirror nuclei, ^{21}Mg will be one of the few accessible $T_z = -3/2$ cases. A particularly interesting case is ^{31}Mg in the context of the «island of inversion» around $N = 20$ and $Z = 12$. Different models are not consistent in the description of this nucleus.

As techniques are refined and studies are extended further from the region of nuclear stability, more stringent requirements are placed on the quality of the ion beams in terms of speed of production, isobaric purity, emittance, energy spread and time structure. Prerequisites for new experiments on light nuclei is the development of new target and ion sources systems at ISOL facilities or ion traps coupled to fragmentation facilities which efficiently slow dawn, capture, accumulate, and cool radioactive beams [106].

2. CALCIUM REGION

The proton magic nucleus Ca is the only element (besides its neighbour K) for which IS measurements have been performed over a full neutron shell, namely, the $\nu 1f_{7/2}$-shell, between ^{40}Ca and ^{48}Ca. The even isotopes in this series, which are all stable, have also been investigated by many other methods which have yielded information on the charge and mass distributions: Coulomb excitation, muon spectroscopy, electron scattering, hadron scattering, and so on. This treasure of data therefore comprises not only precise ms radii but also form factors and their isotopic change. The parabolic-shaped dependence of the ms charge radii for the Ca isotopes obtained by laser spectroscopy, is characterized, firstly, by a maximum in the middle of the shell and, secondly, by the surprising fact that the two double-magic nuclei ^{40}Ca and ^{48}Ca have the same ms charge radius [11, 12]. The very peculiar dependence of the charge radii on the mass number across the $1f_{7/2}$ shell has been ascribed to changes of nuclear deformation different orders [12, 107] whereas the volume of the nuclear charge remains constant for all the Ca isotopes. The recent shell model description [108] includes all configurations of nucleons in the $2s_{1/2}$, $1d_{1/2}$, $1f_{7/2}$ and $2p_{3/2}$ orbits and reproduces very well the characteristic features of the nuclear radii changes of Ca isotopes.

Although the symmetric parabolic behaviour of the Ca radii is qualitatively echoed by the neighbouring odd-Z potassium chain [24], distinct differences include the amplitude of the midshell maximum and the odd–even staggering, which are both much smaller for the potassium chain. Such gross differences are unusual for neighbouring isotope chains [5, 9]. To obtain a fuller picture about nuclear properties in the calcium region it is necessary to have information on nuclear radii trends for other neighbouring isotope chains.

The nearest neighbour of Ca (and K) at the lower-Z side is Ar, and at the higher-Z side are Sc and Ti. The problems related with the laser spectroscopy measurements on these still low-Z nuclei are discussed in detail at the beginning of Sec. 1. For argon, they were met by the method of ultra-sensitive collinear laser spectroscopy described in Subsec. 1.1.1. For Sc and Ti additional difficulties arise due to the refractory nature of these elements. Technical limits connected to the heating required for an efficient release make the conventional ion sources unsuitable for the most refractory elements. Also, total separation times of less than one second are hard to achieve, making it impossible to study very short-lived nuclei. Recently developed high-sensitivity technique [31] involving the cooling and bunching of radioactive ions at the IGISOL (Ion-Guide Isotope Separator On-Line) facility, enables the optical study of refractory elements.

Following the main idea of the present paper, first we will describe the new experimental technique at IGISOL and only then we will go into presentation and discussion of the experimental results on other elements from the Ca region.

2.1. Laser Spectroscopy at IGISOL. In the IGISOL facility at the cyclotron of the University of Jyväskylä (Finland) no ion source in the classical sense is used. The technique involves thermalizing nuclear reaction products by slowing them in a fast flowing jet of helium gas. A significant fraction (1–10%) of the reaction products remain in the 1^+ charge state and these ions are separated from the gas by a skimmer electrode in the jet expansion region. The ions are then electrostatic accelerated to 37–40 keV and injected into a mass-separator (Fig. 9). The advantage of this technique is that it can be applied to any element, including refractory metals, and the extraction time allows beams of ions with half-lives as short as millisecond to be produced without significant loss through decay [53, 109].

A major disadvantage of the IGISOL technique is that the ion beam has a relatively large energy spread (10–150 eV), caused by collisions with gas molecules during electrostatic extraction from the helium. Both the energy spread and the ion yield increase with the skimmer voltage, but the sensitivity of laser spectroscopy at the IGISOL is critically dependent on the quality of the beam. A new method has been developed for increasing the sensitivity of collinear laser spectroscopy. The method utilizes an ion-trapping technique in which a continuous low-energy ion beam is cooled and accumulated in a linear Paul trap and subsequently released as a short bunch [31].

The ion beam cooler-buncher at the IGISOL facility is positioned immediately downstream of the analyzing magnet of the separator. Thus, only a desired fraction of the total output of the separator is cooled and unnecessary space charge limitations are avoided. The device consists of a gas filled rf quadrupole placed on a high voltage platform 100–500 V below the separator potential that is typically 37–40 kV. The ions are thus decelerated as they enter the cooler and are focused into the quadrupole by two cylindrical electrostatic lenses. A technical

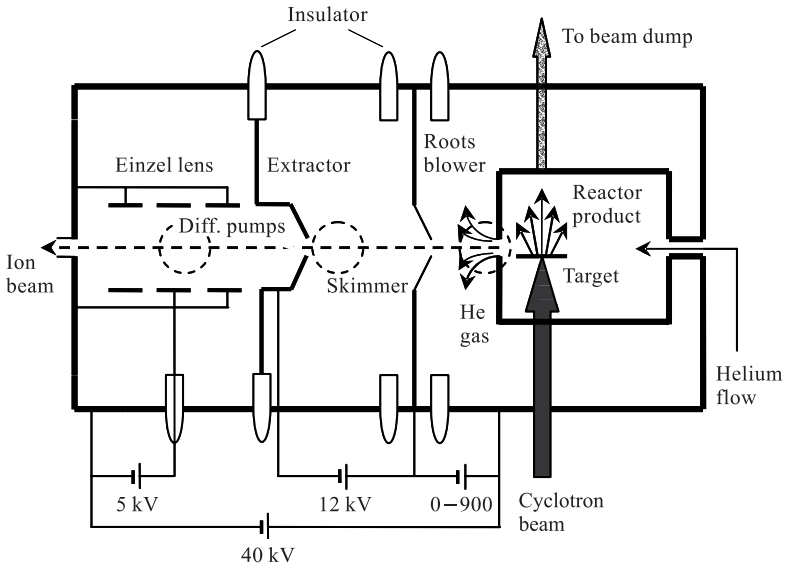

Fig. 9. The IGISOL (Ion Guide Isotope Separator On-Line)

description of the cooler-buncher construction can be found in [110]. The principle of the ion bunching is presented in Fig. 10. The ions are accumulated typically for a few hundred milliseconds ($t_{\rm acc}$). The trap is opened for 100 μs to release the bunch with a width of 10–20 μs. The benefit to collinear laser spectroscopy is diverse. The energy spread of the extracted beam is of the order of 10^{-5} of the total 40 keV energy. At this level the corresponding Doppler broadening of the laser resonance is less than the natural line-width of most allowed atomic (ionic) transitions. The emittance is smaller after cooler, estimated to be 3π mm $\cdot$ mrad resulting in a better spatial overlap between the ion beam and the anticollinear laser beam. Moreover, the overlap is independent of the ion source and isotope separator or ion guide conditions, making the experiment insensitive to drifts in the separator or ion guide conditions. Finally, the bunching capability of the cooler has led to the introduction of a new way of performing laser spectroscopy using bunched ion beams [111].

As the ions are in a short bunch of time width w, the effective measurement time containing all the real events is a fraction $w/t_{\rm acc}$ of the total measurement time. A significant reduction in the photon background can be achieved by electronically gating the photomultiplier signal such that the photon events are only accepted if they arrive while an ion bunch is in front of the detector. This allows a suppression of the background by a factor of $S = t_{\rm acc}/w$, typically

$S \approx 10^4$. The method is applicable to low intensities ~ 50 s^{-1}. The efficiency of the suppression depends on the width of the bunch and the collection time that can be used without incurring losses in the ion flux.

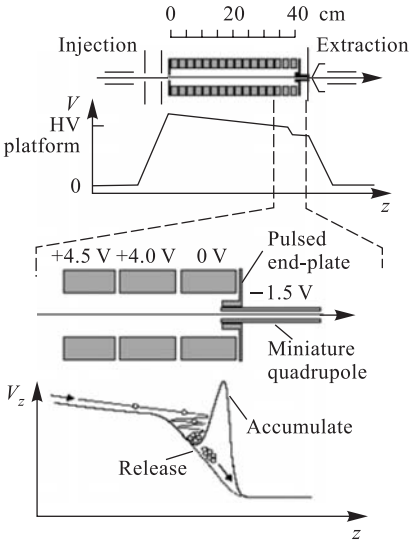

Fig. 10. Schematic principle of the rf-quadrupole ion trap. The ions are accumulated in the trapping zone formed by the rf-quadrupole pseudo-potential V_r in the radial direction and by the dc axial potential V_z in the axial direction with pulsed end-plate voltage at +20 V. To release the accumulated bunch, the end-plate voltage is switched to zero leaving the ions in an axial field gradient of 1.2 V $\cdot$ cm^{-1} that pulses the ions out of the trap. All voltages are relative to the HV platform (from Ref. 31)

The new technique compares very favourably in spectroscopic efficiency to that achieved with the coincidence system [112] when the latter technique is applied to an isobarically pure beam [111, 113]. Its feasibility has been demonstrated by measurements in long isotopic chains containing isotopes away from stability, for example Ti [114] and Zr [115].

2.2. Recent Experimental Results on Nuclear Charge Radii in the $f_{7/2}$ Shell. ***2.2.1. Titanium Isotopic Sequence.*** Data on ms charge radii changes for the stable $^{46-50}$Ti isotopes, covering only the upper half of the neutron $1f_{7/2}$ shell, have been obtained long ago [26, 27] by off-line laser spectroscopy in a collimated atomic beam. The earlier result on ^{44}Ti [116] has shown a continuous increase of Ti charge radii with decreasing mass number. It is very important in the context mentioned above not only to confirm this unusual result but also to continue the measurements across the lower half of the $\nu 1f_{7/2}$ shell ($^{42-45}$Ti).

Recently, study of nuclear ground state properties in a more extended isotopic chain of titanium has been undertaken by the collinear laser spectroscopy at the IGISOL facility with the aim to cover the whole $\nu 1f_{7/2}$ shell [114]. Up to now two additional neutron deficient isotopes are studied: the ^{44}Ti ($T_{1/2} = 49$ y) and the ^{45}Ti ($T_{1/2} = 184.8$ min) produced in the $1n$ and $2n$ channels of the ^{45}Sc$(p, xn)^{46-x}$Ti reactions. The ^{45}Ti yield was of the order of 1500 ions/s, and that for ^{44}Ti, of the order of 100–200 ions/s. The isotope shifts, $\delta\nu^{48,A}$, and hyperfine structure of the Ti isotopes were measured in the transition $d^2s\ {}^4\mathrm{F}_{3/2} \rightarrow d^2p\ {}^4\mathrm{F}_{3/2}$ of the Ti II spectrum with $\lambda = 324.2$ nm.

The data on the charge radii of the $^{44-50}$Ti isotopes is presented on Fig. 11 (Subsec. 2.3). The evolution of the Ti nuclear radii, as the isotopes become more neutron-deficient, shows a generally increasing tendency. A significant difference is observed with the neighbouring Ca isotopes which exhibit asymmetric parabolic behaviour with neutron number. Distinguished ideas could be developed for explanation of the unusual large ^{44}Ti charge radius.

i) In contrast to the other Ti isotope ground states, the ^{44}Ti ground state is predicted to have a dominant cluster structure, in this case composed of a ^{40}Ca core $+\alpha$ particle [117–119] which is not to be expected in the ground states of neighbouring isotopes. This structure would be reflected in an additional increase of the ^{44}Ti charge radius.

ii) Theoretical approaches such as the relativistic mean field (RMF) calculations do provide a valuable framework for understanding charge radii trends. The even Ti isotopes were selected as a particular case for study by Lalazissis et al. [99, 100] and they indeed predict noticeably different behaviour compared with the Ca isotones for both proton and neutron distributions. The calculations show, as is observed experimentally, a monotonic increase in ms radii going from the $N = 28$ shell to below the $N = 20$ shell. The rise is due to the reducing proton binding energies as the proton drip line is approached. The RMF calculations suggest a proton skin forms in isotopes close to the drip line.

2.2.2. Argon Isotopic Sequence. The experimental [30, 41, 104] charge radii evolution in the $^{32-46}$Ar isotopic chain (see Fig. 11) has been described by Klein et al. [30] in spherical Hartree–Fock calculations with the SGII Skyrme interaction from [120]. This interaction reproduces well the single particle energies near ^{40}Ca and their mass dependence up to ^{48}Ca. For argon, the $(\pi 1d_{5/2})$ orbit is essentially closed and the $(\pi 1d_{3/2})$ and $(\pi 2s_{1/2})$ states only can be considered active. As far the neutrons are filling the sd shell, both orbits remain well separated [121]. Therefore, the ground state wave functions are dominated by configuration with a maximum allowed number of particles in the $(\pi 2s_{1/2})$ orbit. When the neutrons begin to fill the fp shell, the two orbits become more and more degenerate inducing strong mixing of the wave functions and thus influencing the evolution of the nuclear charge radius. It has been shown, that the two holes in the $\pi 1d_{3/2}$ orbital in ^{38}Ar are split approximately to one $\pi 1d_{3/2}$ hole and one hole in $\pi 2s_{1/2}$ in ^{46}Ar. Hartree–Fock calculations have been performed with a linear interpolation for the two-proton-hole occupancies between ^{38}Ar and ^{46}Ar [30]. It turns out that moving of the proton hole from $\pi 1d_{3/2}$ to $\pi 2s_{1/2}$ has the effect of increasing the radius. The calculations lead to i) an almost linear increase of the radii between $N = 14$ and $N = 22$ and ii) a relatively larger change from ^{38}Ar to ^{46}Ar compared to the change from ^{40}Ca to ^{48}Ca. As one can see from Fig. 11, this is in agreement with the experimental observation. In addition, the spherical HF predicts quantitatively the absolute value of the charge radii changes $\delta\langle r^2\rangle^{38,39}$ and $\delta\langle r^2\rangle^{38,46}$, but fails to explain the parabolic-like shape and odd–

even staggering of the radii variation between both the neutron shell closures $N = 20$ and $N = 28$.

The spherical HF is justified by the fact [122] that nuclei, whose mass numbers do not deviate very much from the closed shell configuration, stay at least in their ground state spherical symmetric. Filling more nucleons into the shell, one enters a region in which nuclei undergo rapid changes in deformation, reaching its maximum value in the middle of the shell. Hence, part of the discrepancy between theory and experiment can be attributed to quadrupole core polarization phenomenologically represented by the quadrupole deformation $\langle\beta^2\rangle^{1/2}$. As shown in [104], the corresponding shape correction drastically changes the smooth trend of ms charge radii predicted by spherical HF and leads to a structure very similar to the experimental one. Thus, a clear correlation between changes of the nuclear radii for even–even argon isotopes and the phenomenological $\langle\beta^2\rangle^{1/2}$ values is found.

2.3. Systematics of Nuclear Charge Radii in the Calcium Region. The investigation of Ar ($Z = 18$) isotopes with neutron numbers between $N = 20$ and $N = 28$ together with the old data for K [24], Ca [11, 12, 123], and Ti [26, 116] and the recent laser spectroscopy experiments on ^{44}Ti and ^{45}Ti [114] may serve as a cornerstone for a more global systematics of the charge radii in the region around the $Z, N = 20$ and $N = 28$ shell closures, i.e., in the calcium region. Three types of experimental data will be summarized here: isotopic and isotonic variations of the nuclear charge radii and, additionally, the odd–even staggering effect. The isotopic and isotonic systematics is obtained based on the combined analysis of two types of experimental data [9]: radii measured from electronic scattering and muonic atom spectra and radii changes determined from optical isotope shifts. Figure 11 displays the dependence of the ms radius $\langle r^2\rangle$ on the neutron number N and Fig. 12 — the dependence on the proton number Z. The following characteristic features are evident.

The slope of the isotonic curves, $\langle r^2(Z)\rangle$, is considerably steeper than that of the curves $\langle r^2(N)\rangle$. This can be understood in terms of the additional Coulomb interaction between protons compared with the interaction between neutrons, which leads to a larger increase in $\langle r^2\rangle$ when protons are added as compared to when neutrons are added. This feature is common for the global charge radii systematics [9].

The second characteristic feature is connected to the magic numbers. As shown by the gross nuclear radii systematics [9], the slope of the $\langle r^2(N)\rangle$ and $\langle r^2(Z)\rangle$ curves at all spherical shell closures with $N \geqslant 28$ changes from a small decrease or increase below to a steep increase above. The same refers to the charge radii behaviour in the calcium region close to the neutron magic number $N = 28$ (see Fig. 11). This well-known effect, arising from a monopole polarization of the proton core by the additional valence neutrons, is discussed and explained in a number of papers, e.g., [124, 125]. Unfortunately, no conclusion

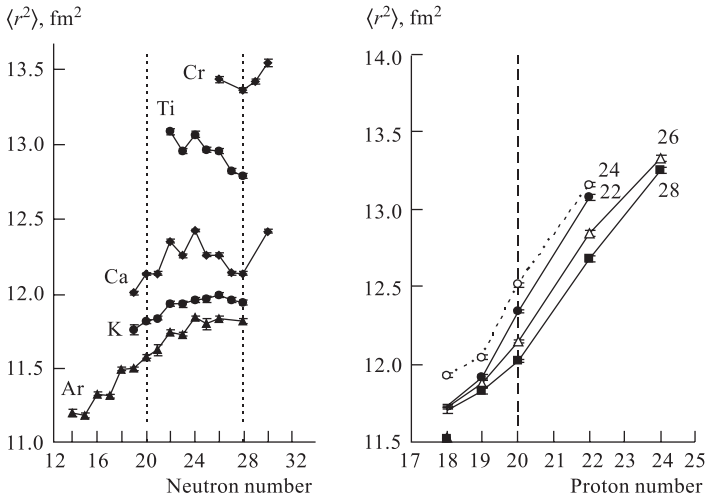

Fig. 11. Mean square nuclear charge radii versus neutron number

Fig. 12. Mean square nuclear charge radii versus proton number. The isotonic curves with $N = 20$, 24, 26, and 28 are presented. To see the $\langle r^2 \rangle$ evolution better, the curves are shifted with 0.1 fm^2 with respect to the one for $N = 22$ in such a way that the relative curve position is kept

could be made on the isotonic behaviour in the vicinity of $Z = 28$, since there is no experimental data for the upper $1f_{7/2}$ proton shell.

On the contrary, the sequential addition of neutrons (Fig. 11) or protons (Fig. 12) going from the sd- to the $f_{7/2}$-shell results in an almost linear increase of the successive charge radii. This is more pronounced in the isotonic charge radii dependence, i.e., at the proton shell closure $Z = 20$. At the neutron shell closure $N = 20$ analogous phenomenon has already been observed for sd-shell nuclei: heavy Na [20, 21], Mg [22, 23], and Ne isotopes [44]. There the situation is caused by the abnormal ratio of protons and neutrons in the upper part of the sd shell, which manifests itself in the appearance of new regions of deformation and new islands of inversion. However, this is not the case in the calcium region where the number of neutrons and protons around $N = 20$ is nearly equal. Nevertheless, the absence of pronounced changes of $\langle r^2(N) \rangle$ when the magic number $N = 20$ is crossed is the most striking characteristic of this systematics indicating the disappearance of any shell effect. This can be explained by a cancellation of the monopole polarization and the quadrupole polarization on the proton core under successive addition of valence neutrons [12, 30]. As shown by [107], higher order polarizations associated with the low-lying collective states of different isotopes play an important role, too.

An unusual behaviour of the isotonic $\langle r^2(Z)\rangle$ curves at the proton shell closure $Z = 20$ is observed (Fig. 12). For $N = 20$ to 24 no kink is seen crossing the magic proton number. A slight indication of a slope change at $Z = 20$ appears only in the upper half of $\nu 1f_{7/2}$ shell. Such effect in the isotonic $\langle r^2(Z)\rangle$ trend is observed for the first time. It may or may not be interpreted as an absence of a shell effect at $Z = 20$. However, different characteristics in the behaviour of the isotopic change of the charge radii below and above $Z = 20$ are observed (see below). These can be regarded as shell closure effects. Thus, the unusual $\langle r^2(Z)\rangle$ trend at $Z = 20$ remains so far unexplained.

The third feature is the shape of the $\langle r^2(N)\rangle$ curves for adjacent Z in Fig. 11 and of the $\langle r^2(Z)\rangle$ for adjacent N in Fig. 12. All curves in Fig. 11 show a parabolic-like dependence of the charge radii on the neutron number. Nevertheless, in opposition of what is expected from the gross nuclear radii systematics, the similarity concerns only the parabolic-like shape. The well pronounced symmetric parabolic shape in the calcium case is not reproduced by the neighbouring elements. Moreover, the shape asymmetry for elements with $Z > 20$ and with $Z < 20$ is in the opposite direction. Explanations of these trends are given in the previous subsections of Sec. 2.

The isotonic nuclear radii in Fig. 12 have more similar behaviour for adjacent Z: the $\langle r^2(Z)\rangle$ curves are almost parallel. $\langle r^2(Z)\rangle$ increases only slightly with N as far as the $f_{7/2}$ midshell at $N = 24$ is reached and then decreases again. Obviously, this is due to the opposite asymmetry of the isotopic charge radii trends in both sides of the $Z = 20$ shell closure.

A suitable approach for discussing the radii behaviour in the Ca region from the common point of view is the Talmi–Zamick-formula [126, 127]. It is proposed in order to retain the essential physical features observed in Ca isotopes. It assumes a simple model mixing to the shell model states of some other excited states in such a manner that $\nu f_{7/2}^n$ couples to an excited, presumably deformed core state. The changes of the ms charge radius caused by adding n particles to the $\nu 1f_{7/2}$ shell is given by the expression [126]

$$\delta\langle r^2\rangle^{20,20+n} = \langle r^2\rangle^{20+n} - \langle r^2\rangle^{20} = nC + \frac{n(n-1)}{2}\alpha + \left[\frac{n}{2}\right]\beta, \qquad (11)$$

where $[n/2] = n/2$ for even n and $[n/2] = (n-1)/2$ for odd n. It considers one-body (parameter C) and two-body (parameters α and β) interactions of the added particles with the core. As proposed, the formula applies to the ms charge radius of a nucleus with only neutrons (or only protons) outside a closed shell. According to [128], the Zamick formula can be extended to all $1f_{7/2}$ nuclei, including those with both neutrons and protons outside closed shells. Indeed, formula (11) fits the experimentally measured ms charge radii of Ar, K, and Ca isotopes very well, but in some extends at the cost of a stringent interpretation

(see, e.g., [3, 12, 25]). However, for Ti, similarly to the K, Ca, and Ar cases, this approach predicts a decrease of the charge radii in the neutron deficient part of the $\nu 1f_{7/2}$ shell which is in contradiction with the experimental data for ^{44}Ti. Let us note, that Eq. (11) describes $\delta\langle r^2\rangle$ only as a function of the number of valence neutrons and does not take explicitly into account collective effects like nuclear deformation.

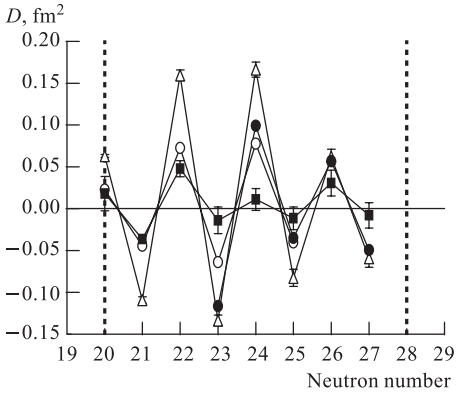

Fig. 13. The odd–even staggering D for the odd-N and even-N isotopes: Ar (○), K (■), Ca (△) and Ti (●)

The fourth interesting feature is the odd–even staggering (OES) in the curves $\langle r^2(N)\rangle$ shown in Fig. 13. Note that the staggering effect also appears in the isotonic systematics in Fig. 12. However, there the only odd-Z isotopes available are with $Z = 19$. In the normal OES the charge radius of a nucleus with an odd number of neutrons is smaller than the average radius of its two neighbours with even neutron numbers. It may be transparently described in terms of the difference D between the radius of an odd (even)-N isotope and the mean value of the radii of its even (odd)-N neighbours which is equivalent to

$$D = \delta\langle r^2\rangle^{N_0,N} - \frac{1}{2}\left(\delta\left\langle r^2\right\rangle^{N_0,N-1} + \delta\left\langle r^2\right\rangle^{N_0,N+1}\right). \tag{12}$$

Here N_0 is the neutron number of the reference isotope. The main contribution to the odd–even effect comes from quadrupole and higher order even core polarization which leads to linear and quadratic terms in n. As can be seen from Eq. (11), the OES in the charge radii is described by the parameter β: $\beta = 0.106(21)$, 0.047(18), 0.223(51), and 0.159(43) fm^2 for Ar, K, Ca, and Ti, respectively. These values are in very good agreement with the observed OES. It is clearly seen, that away from Ca the odd–even staggering decreases. The largest decrease is at the odd-Z nucleus K. Whether or not this is a pairing effect in the even-Z chains is a question that deserves closer attention than we are able to give in this paper. At the other hand, the D value for even-Z neighbours of Ca is essentially larger than for K, but smaller than in the calcium case. This may be prescribed to the stabilizing role of the closed proton shell at Ca for which the Talmi calculation [129] is valid with the best approximation.

The mean field calculations, which usually aim to describe nuclear parameters and radii over a large region of nuclear masses and charges, cannot account for the details of the IS in calcium region. The dependence of $\langle r^2\rangle^{1/2}$ on A is usually

featureless. Some of the approaches, however, are able to account at least for the near equality of the charge radii in ^{40}Ca and ^{48}Ca, and for the general trend of the Ti and Ar charge radii between $N = 20$ and $N = 28$. To this category belong, e.g., calculations based on the HF method with Skyrme interactions [130] and RMF method [100]. The best description of charge radii of the Ca isotopes in the $f_{7/2}$ shell is in the framework of the shell model using cross-shell proton-neutron correlation [108]. The self-consistent RMF approach of [99, 100] predicts in the case of Ti a continual increase in the charge radius going from $N = 28$ to the $N = 20$ shell closure. The RMF calculations of [99, 100] do not describe a noticeable kink in the charge radii systematics at $N = 20$ for any isotope chain. This prediction is in agreement with all available experimental data which cover the Ar [30], K [24], and Ca [11, 12] chains.

2.4. Summary. Section 2 gives an overview of our present understanding of the charge radii in the calcium region emphasizing the successes of the experimental laser spectroscopic techniques of the last years as well as the difficulties faced by the shell model and the modern RMF theory.

The charge radii trends of Ar, K, Ca, and Ti isotopes across the $\nu 1f_{7/2}$ shell are compared. Although a parabolic-like dependence of charge radii on neutron number is evident in all four chains, the differences between the chains are greater than one would expect for such a restricted mass region. As more experimental data become available, it is the behaviour of the Ca chain radii that is seen as anomalous in this region. The strongly-magic proton number, $Z = 20$, of Ca seems to reinforce the $N = 20$ and 28 closures, leading to reductions, particularly in the neutron, but also proton radii.

Four effects are distinguished in the isotopic and isotonic nuclear radii systematics in this region which present new challenges for the theory. Of course, to obtain a fuller picture about nuclear properties in the calcium region it is very interesting to have additional experimental information. Here we stress the importance of some further investigations:

• A continuation of the optical investigation of Ti isotopes to the lighter ^{43}Ti and especially to ^{42}Ti at the $N = 20$ shell closure which is expected to provide a stringent test of the theoretical models.

• Information on nuclear radii changes in an isotopic chain of scandium, the second neighbouring odd-Z element of calcium, which will give a more definite picture of the role of the pairing effect of even-Z isotopes.

These are upcoming experiments, planned to be carried out with the laser spectroscopy setup at the IGISOL facility [131]. We note in addition the following:

• It would be of great importance to extend the region of investigated elements to higher Z up to the proton magic number $Z = 28$ in order to obtain more detailed information about the isotonic behaviour of $\langle r^2 \rangle$ in the $1f_{7/2}$ proton shell. For these nuclei the proton drip line is accessible just in the $1f_{7/2}$ shell.

Due to the small binding energies of nuclei close to the drip lines, one expects a lowering of the nuclear density, novel type of shell structures [132], or presently unknown unusual collective modes.

• On the contrary, investigations of the isotope chains covering $\nu 1f_{7/2}$ shell for elements with $Z < 18$ will move us close to the neutron drip line of these elements. In particular, the role of the $N = 28$ gap in the exotic neutron rich isotopes with $Z = 14$, 16, and 18 is widely discussed in the theory [121, 130]. In general, one predicts that the $N = 28$ shell closure persists, even if eroded by the large neutron excess.

Finally, a continuation of charge radii measurements to the neutron rich side of the isotopic sequences with $N > 28$ is also necessary to give a link to the charge radii development toward the next magic numbers $N = 50$.

3. TOWARDS THE MEDIUM-Z REGION

From the point of view of nuclear structure investigations by laser spectroscopy traditionally interesting are regions (i) where well-deformed nuclei can be found or their deformation drastically changes and (ii) around nuclear shell closures or around double magic nuclei. Both cases are of special importance for very neutron rich nuclei.

In the first case, these are regions of nuclei where some peculiarities in the behaviour of nuclear shape and size can be observed and explanations of them are good testing points of nuclear models. Some of these regions are already well investigated, e.g., shape transition of the rare-earth elements around $N = 88$, shape transition and shapes coexistence in the high-Z nuclei in the osmium to lead region [45, 133, 134]. In the known deformation region around $N = 90$ the change in a nuclear shape is quite different for different elements: there is a sharp jump in the β-stability valley (isotopes of Nd, Sm, Eu, Gd) and a smooth growth outside it (neutron-rich isotopes of Ba and neutron-deficient isotopes of Yb) [4]. In the last case the increase of the quadrupole deformation occurs with decreasing the octupole deformation.

However, the deformation region between $N = 60$ and $N = 82$ for neutron-rich nuclei remains still poorly investigated. It is only known that there is a sharp jump in quadrupole deformation at $N = 60$ for isotopes with $Z < 40$. It manifests itself by a strong change in their charge radii, e.g., in Sr [135], and reduced probabilities of electric quadrupole transitions [136]. But it remains temporarily unclear what will happen in nuclei just around $Z = 40$ (e.g., Y–Mo). There exist several theoretical models which predict interesting properties of nuclei in this region. According to some of them [137] around the middle of the region ($N \approx 66$) a sign change of the quadrupole deformation parameter is to be expected. One of the most interesting cases seems to be the Zr-isotope chain in which a shape transition is predicted to occur at different neutron numbers.

Progress in the field is the recent investigation of a long isotopic chain of Zr [113, 115, 138]. The data will be discussed in Subsec. 3.1.

One of the goals of modern nuclear physics is to understand the structures of nuclei far from the line of stability and at extremes of isospin. Thus far such studies have largely dealt with the light nuclei for which radioactive beams have been available at facilities such as ISOLDE (CERN) [139], RIBS (Riken) [140], IGISOL (Jyväskylä) [141], DRIBs (Dubna) [142], and TRIUMF/ISAC (Vancouver) [143]. As pointed out in Sec. 1, early experiments have led to the identification of novel structures of which the halo is the best known after its identification in ^{11}Li. The efforts to extend such investigations to heavier nuclei have been advanced in the theoretical study of neutron rich nuclei across the whole mass range. In the last decade the extension of nuclear techniques far off stability permitted neutron-rich fission fragments of medium-Z elements (in the region from Zn to Ce) to be produced with sufficiently high yields.

Let us give an example. A new project «Dubna Radioactive Ion Beams» (DRIBs) is now in the stage of realization at the Flerov Laboratory of Nuclear Reactions, JINR (Dubna). According to the project a wide range of neutron-rich isotopes of different elements can be produced in ^{238}U(γ, f) reaction. A uranium target will be irradiated by the bremsstrahlung with maximum energy of 25 MeV on the electron beam with intensity of 20 μA of the MT-25 microtron. The total fragments yield from 100 g U target can be of the order of 10^{11} s^{-1}. The yields (independent and cumulative) of the ^{238}U photo-fission have been calculated [29] for a number of elements. It is shown that the isotopic distributions are wide enough; they include up to 10 isotopes with relative yields of more than 1% of the maximal one. The yields of some fragments are presented in Table 3. These fragments are interesting from the point of view of their nuclear structure having number of protons or neutrons close to the magic numbers, large quadrupole deformations, and unusual mode of radioactive decay. The predicted yields are large enough for many high-sensitivity laser spectroscopic techniques.

This example illustrates the promise held by the development of the nuclear facilities for expanding the investigation of nuclear structure in new regions of exotic nuclei. Two peculiarities of the neutron-rich fission fragments are very important: low neutron binding energy (< 5 MeV) and high β-decay energy (> 5 MeV). These lead to a completely new situation in the decay characteristics and level properties of the fission fragments compared to those of the nuclei from the β-stability valley.

The nuclear parameters which can be deduced by laser spectroscopy determine the nucleon configurations of ground and isomeric states, the size and shape of a nucleus; they identify the levels and their nature. It is very important to establish how these nuclear properties are changed with increasing neutron excess and when the neutron drip-line is reached. The most interesting regions and directions of investigation of fission fragments are the following:

Table 3. **Some characteristics of the photo-fission fragments of ^{238}U**

Fission fragments	Peculiarities	Y, $1/f$	Y, $1/s$ (DRIBs)
^{80}Zn	Neutron shell closure $N = 50$	10^{-6}	10^{5}
^{81}Ge	Neutron shell closure $N = 50$	$3 \cdot 10^{-5}$	$3 \cdot 10^{6}$
^{131}In	Neutron shell closure $N = 82$	10^{-3}	10^{8}
^{132}Sn	Double magic nuclei $Z = 50$, $N = 82$	$3 \cdot 10^{-3}$	$3 \cdot 10^{8}$
^{134}Sn	2 neutrons over closed shell	$8 \cdot 10^{-4}$	10^{7}
^{100}Zr	Beginning of deformation region	10^{-2}	10^{9}
^{104}Zr	Strongly deformed nuclei	$5 \cdot 10^{-4}$	$5 \cdot 10^{7}$
^{160}Sm	Strongly deformed nuclei	10^{-4}	10^{7}
^{134}Sb	Delayed two-neutron emitter	10^{-6}	10^{-5}
^{140}I	Delayed α emitter	10^{-5}	10^{6}

• Nuclei near neutron shells closures: $N = 50$ (isotopes of Zn, Ge, Ga) and $N = 82$ (isotopes of Cd, In, Sn). The regularity of charge radii changes in isotope sequences for the β-stability valley or for neutron-deficient nuclei is well known: nuclides with a magic neutron number have the smallest radius (or the most compact shape). It will be very interesting to clear if this trend remains at the transition to very neutron-rich nuclei. Here it is very important to determine the parameters of lower single particle states at the end of the filled shell and at the beginning of the next.

• Shape isomers in fission fragments. In some nuclei there exist excited states with unusual large quadrupole deformation (the deformation parameter $\beta \geqslant 0.6$). In nuclei with $Z \geqslant 92$ (see Sec. 4) these states are isomeric (spontaneously fissioning isomers [144]). In other regions of nuclei excited rotational bands are observed with an unusual large quadrupole deformation (supper- and hyperdeformations [145, 146]). However, the lowest states of these bands have not been detected up to now. Probably these states are isomeric and their study is of great interest. One can identify such states by the abnormal large isomeric shift of the optical lines, caused by the large deformation difference between ground and isomeric states. Among the fission fragments such states have been predicted for nuclei around ^{78}Zn and ^{114}Ru.

• Nuclei with difference in spatial distribution of electrical charge and nuclear matter. The large excess of neutrons in fission fragments can result in an essential difference in the spatial distribution of protons and neutrons. Usually information about this difference is obtained by a comparison of the cross sections for elastic scattering and the charge-exchange reactions induced by such nuclei. Experiments of this kind are planned to be carried out on beams of accelerated fission fragments in the DRIBs project. But it is possible to get similar information by laser spectroscopy. The method to be used is based on the Bohr–Weisskopf

effect [147] — the influence of the spatial distribution of the nuclear magnetic moments on the hyperfine splitting of atomic levels. The deviation of the ratio of the gyromagnetic factors from the ratio of the magnetic dipole constants gives information about the neutron distribution radius.

These examples show how wide can be the field of activity in the study of the nuclear structure of neutron-rich nuclei. Below (Subsec. 3.2) we will focus on a selected case of laser spectroscopic investigation: the proton magic ($Z = 50$) tin neutron-rich isotopes around neutron magic number $N = 82$.

3.1. Shape Transition Regions. The development of the IGISOL technique, involving the cooling and trapping of radioactive ions [31], facilitates the optical study of refractory elements. Recently this method has been used to explore part of the refractory region around $N = 50$, with the determination of the changes in nuclear ms charge radii, $\delta\langle r^2\rangle^{90,A}$, magnetic moment, μ, spectroscopic quadrupole moment, Q_s, and nuclear spin, I, for the ground states of the neutron-deficient isotopes of zirconium, $^{87-89}$Zr, and also the two long-lived isomers ^{87m}Zr ($T_{1/2} = 14.0(2)$ s) and ^{89m}Zr ($T_{1/2} = 4.16(2)$ min). The radioactive Zr isotopes were produced via ^{89}Y(p, xn)$^{90-x}$Zr fission-evaporating reaction. For each of the studied masses yields of few thousand ground-states Zr ions/s and isomer production rates of ~ 300 ions/s have been obtained.

Further, the measurements have been continued towards the region of zirconium fission fragments from ^{96}Zr to ^{102}Zr. The neutron-rich $^{96-102}$Zr isotopes were produced by the fission of uranium, induced using 3.5 μA of 25 MeV H^+. A production of ~ 3000 s^{-1} was achieved for the most strongly produced ^{100}Zr. The minimal studied ion rate was ~ 500 s^{-1}. A detailed description of the experimental conditions, data acquisition and analysis may be found in [113] for the neutron-deficient and in [115] for the neutron-rich Zr isotopes.

The evolution of the ms charge radii between $N = 44$ and $N = 62$ as a function of neutron number is characterized by: i) the smallest value at the $N = 50$ neutron shell closure where the nucleus is approximately spherical in shape; ii) rapid increase on either side of the magic number and iii) a jump in the charge radius at $N = 60$. The latter can be attributed to the predicted shape change in this region, which originates from the breakdown of the stabilizing semimagic proton shell closure at $Z = 40$ [150]. This sudden onset of strong deformation has already been observed in the gamma ray spectroscopy [151] of isotope chains in this region of the nuclear chart.

To prove the validity of the different theoretical predictions [98, 100], the quadrupole nuclear deformation in the Zr isotopic sequence has been analyzed and deformation parameters have been extracted from the ms charge radii and the spectroscopic quadrupole moments [138]. In Fig. 14 they are compared with the values of $\langle\beta_2^2\rangle^{1/2}$ obtained from $B(E2)$ measurements [136]. Below $N = 50$, the agreement between the static (from Q_s) and dynamic (from $\delta\langle r^2\rangle$) deformation parameters is poor. The large dynamical contribution to the deformation suggests

that the Zr nuclei have soft, vibrational shapes below $N = 50$. In the region beyond the $N = 60$ shape change, where strong quadrupole deformation sets in, the deformation parameters derived by different methods become more compatible. This agreement suggests that the nucleus takes on a rigid, statically-deformed shape above $N = 60$, which are consistent with gamma-ray observations of deformed rotational bands in this region. In addition, these conclusions are supported by the systematics of the first excited 2^+ state energies, and the energy ratios of the first excited 4^+ and 2^+ states $E(4^+)/E(2^+)$ [138].

In the transitional region, $50 < N < 60$, it is more difficult to draw conclusions about the behaviour of the nuclear shape, due to the discrepancies between $B(E2)$ and ms charge radii measurements. They are due to model approximations in the analysis, and may indicate that there are significant changes in the surface diffuseness between isotopes. Similar discrepancies in the strontium chain have been considered by Mach et al. [152], who concluded that the effect of octupole vibrations could account for the differences.

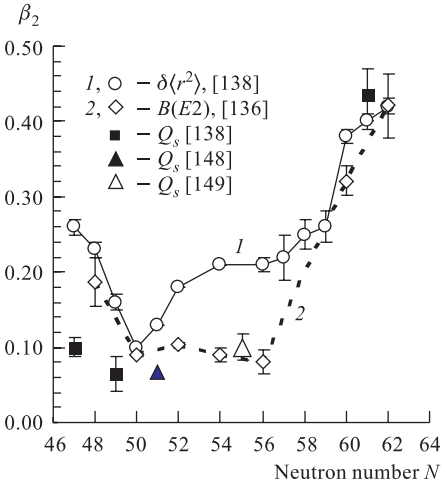

Fig. 14. Variation of the absolute value of the quadrupole deformation parameter $|\beta_2|$ with neutron number [138]. The source data is shown in the inset of the figure. In all cases the well-known standard methods have been used (see, e.g., [3]) to extract the $|\beta_2|$ from the corresponding quantities: $\delta\langle r^2\rangle$, $B(E2)$ and Q_s

Urban et al. [151] proposed the coexistence of a spherical configuration, which becomes weakly deformed with increasing N, and a deformed configuration, which first appears as a weakly deformed excited state at $N = 57$ and becomes steadily more deformed up to a point of saturation at $N \sim 62-64$. Shape coexistence is predicted to extend up to $N = 63$, with the deformed configuration becoming the ground state at $N = 60$ and producing the observed shape change. As shown in [138], the experimentally observed trend in the ms charge radii appears to be consistent with this idea of a gradual increase in deformation.

The combination of the $N = 56$ and $Z = 40$ subshell closures is believed to be responsible for delaying the onset of deformation in Zr [153], thus producing the rapid shape changes which are observed.

3.2. Neutron-Rich Tin Isotopes. ***3.2.1. Advance in Experimental Technique.*** Laser spectroscopy at ISOLDE is an outstanding way of studying nuclear

deformation and structure to the limits of stability. Complementing the collinear laser spectroscopy studies long pursued at ISOLDE [34], the COMPLIS (COllaboration for spectroscopy Measurements using Pulsed Laser Ion Source) concentrates on elements which are not accessible at ISOLDE ion beams. The COMPLIS setup has been designed to perform high-resolution Resonance Ionization Spectroscopy (RIS) on a pulsed secondary atomic beam of daughter nuclides produced by laser desorption. The COMPLIS experimental setup has been described in detail by Sauvage et al. [154]. Here we lay stress on the COMPLIS modification for laser spectroscopic measurements of charge radii in the vicinity of the double magic ^{132}Sn.

The neutron-rich tin nuclei have been obtained at ISOLDE by fission reactions, in a uranium carbide target, induced by the 1 GeV proton beam delivered by the CERN-PS-Booster. This target is associated either with the hot plasma ion source designed for ionization of low volatility elements or with a LIS (Laser Ion Source) tuned for tin. It must be noted, that with the hot plasma ion source, many other elements are ionized like In, Cd, Sb, Te, I, and Cs, and for instance at $A = 132$ tin represents only 0.24% of the observed nuclei. With the LIS, Cs is also ionized, probably by surface ionization mechanism and his yield is high. These various isobaric contaminations have to be taken into account to determine which ion source has to be used. The choice depends on the laser spectroscopic setup.

Three setups are available at ISOLDE: COLLAPS (Subsec. 1.1), COMPLIS and the LIS [155]. The LIS has excellent efficiency due to its high laser repetition rate (10 kHz); the optical resolution (some GHz) gives Z selectivity for most elements but is not high enough to perform isotope shift measurements in the tin nuclei. COLLAPS [156], designed to perform collinear laser spectroscopy on fast atomic beams, has a high frequency resolution (~ 60 MHz) but works best with isobar-free beams, which excludes the use of the hot plasma source. But even with the LIS, the great amount of Cs isobars could give rise to a fluorescent light and thus to a continuous background noise reducing the detector sensitivity. COMPLIS, designed originally for high resolution studies on refractory daughter elements, was not an obvious choice for experiments on tin. However, it is in fact competitive, since the hot plasma ion source, whose Cs yield is lower than of the LIS, can be used. Up to now, the only experimental data from laser spectroscopy on the neutron rich Sn isotopes have been obtained using COMPLIS.

For the tin study, the experiment is performed as follows [157]. The radioactive tin isotopes produced as described above are extracted at 60 kV and mass separated by the Ground Purpose Separator (GPS) of ISOLDE. The ions enter the COMPLIS beam line, are slowed to 1 keV and are thus deposited on the first atomic layers of a rotating graphite substrate. Once the amount of the collected atoms is optimum (the collection time depending on the half-life of the isotope to be studied) they are desorbed by a Nd:YAG laser and selectively ionized by a

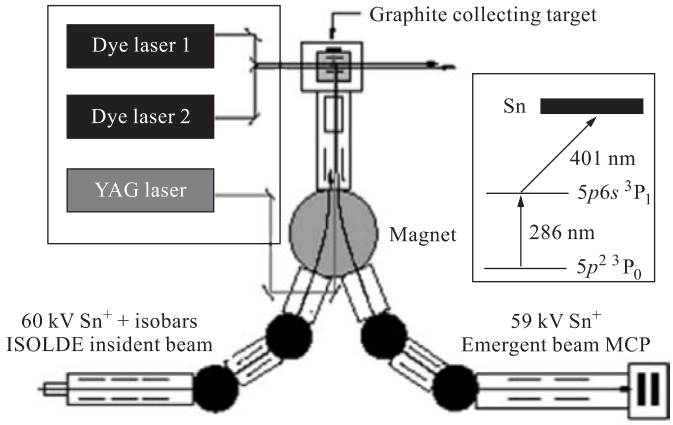

Fig. 15. The COMPLIS experimental scheme used for tin [157]

set of two pulsed, tunable dye lasers where the first-excitation step at 286.3 nm ($5s^2 5p^2\ ^3\mathrm{P}_0 \rightarrow 5s^2 5p6s\ ^3\mathrm{P}_1$) is obtained from frequency doubling. The ions are finally detected with time-of-flight identification using a microchannel plate detector. This experimental setup is shown in Fig. 15. The frequency scan over the hyperfine structure of a given isotope is made as follows: after a sufficient collection time, the desorption of the tin atoms is made over the entire collection spot on the slowly rotating target at a given frequency step. After the desorption is complete, a new cycle of implantation-desorption is run at an advanced frequency step. Whenever the laser frequency corresponds to a hyperfine transition, the desorbed atoms are excited and ionized by the other fixed laser frequency. The number of counted ions at the detector is directly proportional to the intensity of the hyperfine transition. With this apparatus, the efficiency of about 10^{-6} has been obtained with a resolution of 170 MHz.

3.2.2. Radii Near the Doubly Magic Shell at ^{132}Sn. The doubly magic nuclei are of great interest in nuclear physics because their properties (e.g., binding energy, neutron separation energy, radii) are the basis of the parameterization of the effective interactions used for mean-field and RMF calculations [158–164]. In parallel, numerous new and accurate results were obtained making systematic data available along isotopic series from light to heavy nuclei. This motivated many theoretical works in particular to improve the parameters of the effective interactions currently used. The goal of these theoretical studies is to define an effective interaction valid not only along the stability but also for exotic nuclei. The proton-magic tin isotope series contains the doubly magic nucleus ^{132}Sn which is located far from stability. $\delta\langle r^2\rangle$ curves have been calculated for neutron-rich tin isotopes and the predictions depend on the type of calculations

(see [157] and reference therein). The most important question which has to be answered experimentally is: will the $\delta\langle r^2\rangle$ exhibit a slope change at ^{132}Sn as it does for the double magic ^{208}Pb?

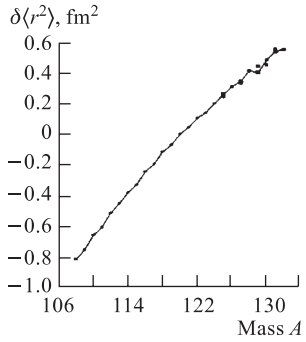

Fig. 16. Development of the charge radii changes in the tin isotope sequence according to [157]. Data for $A = 108$–124 are taken from [165] and recalculated using parameters from [166]

A compilation of the nuclear charge radii changes in the tin isotope chain from $A = 108$ to 132 is shown in Fig. 16. The new COMPLIS data cover the range from $A = 125$ up to 132 and include not only the ground but also some isomeric states. The main remarkable thing that can be seen in Fig. 16 is the appearance of a plateau at mass 131. This suggests the emergence of a neutron skin at $A = 130$ and beyond but additional experimental data are needed to confirm this hypothesis. The $\delta\langle r^2\rangle$ of the even isotopes can however be compared with the existing mean-field calculations. Most of them are not as far from the experimental values (see [157]) but the appearance of the plateau is not predicted. Once more, experimental data on ^{134}Sn are necessary to definitely constrain the models.

A second phenomenon that must be pointed out is a larger odd–even staggering than for the lighter masses which is moreover, inverted. Theoretical data are waited on the odd isotopes to try to explain this unexpected behaviour. Moreover, from the A and B hyperfine constants of the excited atomic state, one can extract the magnetic and quadrupole moments of each isomer and odd isotope. The data are under analysis and the extracted experimental values will be compared with calculations assuming a given nuclear orbital [157].

3.3. Summary. Two topical examples are given showing the progress of the new laser spectroscopic techniques (IGISOL system with an ion cooler/buncher and COMPLIS setup) in the field of neutron rich medium Z element. Here we summarize the main results and discuss the necessity of some additional experiments as well as some problems associated with them.

• The sequence of Zr isotopes ranging from the neutron deficient isotopes with $N < 50$ to the neutron-rich ^{102}Zr at $N = 62$ has been investigated and new information about the poorly investigated shape transition region around $N = 60$ has been obtained. Future optical measurements of ^{93,95}Zr, yielding static ground state deformation parameters, will give a better indication of the systematics of the transition region, $50 < N < 60$. Plans are also in place to study the neutron-deficient and neutron-rich isotopes of yttrium ($Z = 39$), which will further improve the systematics of the $Z \sim 40$ region [138].

• Progress in the study of very neutron-rich nuclides is rather slow [167]. Yet, interesting new data have become available in some places, as, e.g., near the crossing of magic number of protons and neutrons at ^{132}Sn. The success is due to the laser spectroscopy measurements on neutron rich tin isotope from $A = 108$ to 132 at the COMPLIS experimental setup. However, the behaviour of the charge radii beyond the double magic ^{132}Sn remains an open question. Improvement and optimization of the COMPLIS setup are needed to extend the measurements towards higher A. For example, the ^{134}Sn yield is $\sim 10^6$ s^{-1}, the Cs isotopes are ~ 100 times more produced and the half-life of ^{134}Sn is very short ($T_{1/2} = 1.1$ s). Under these conditions, no accumulation of ^{134}Sn is possible and the step-by-step running mode cannot be used. Therefore the laser measurement has to be performed simultaneously with the collection. This requires an essential modification of the COMPLIS setup.

In addition:

• Isotope shifts for the neutron-rich ^{146,148}Ce were measured [168]. The most striking feature of the shape change in Ce isotopes is a smoothly developing shape change in the $N = 88$, 90 region. This shows clearly an intermediate behaviour through the $N = 88$ region for the intermediate Z region ($56 < Z < 60$). Thus, more details concerning the shape transition region at $N = 88$ have been revealed. Studies of the neutron-rich isotopes are planned and aim to extend these measurements into a region of potential octupole deformation [3, 10].

4. TOWARDS SUPERHEAVY NUCLEI

Above uranium, the information on nuclear ground state properties from laser spectroscopy is scarce since these elements are not available at ISOL facilities. The investigation of atomic, chemical and nuclear properties of heavy elements, especially with charge $Z > 100$, is a real challenge. Isotopes of such elements can only be produced by fusion reactions in heavy-ion collision or by transfer reactions using radioactive targets. Gas-filled recoil mass separators or velocity filters are used in the case of fusion reactions. The production yields are sometimes only a few atoms per week [169]. Their lifetimes are short, occasionally only of the order of millisecond.

Moreover, a specific problem of atomic spectroscopy of heavy actinides exists in the generally not known atomic level schemes. Theoretical predictions are difficult because of the many body nature of these elements and strong relativistic effects. The latter originates from shrinkage of the wave functions of inner shell electrons which, in turn, influence the chemical properties of these elements and the binding energy of the valence electrons. In the actinide region these are the $5f$, $6d$, $7p$, and $7s$ orbitals. Therefore, a direct approach to investigate relativistic effects may be to study first ionization potential (IP) or, even better, the atomic

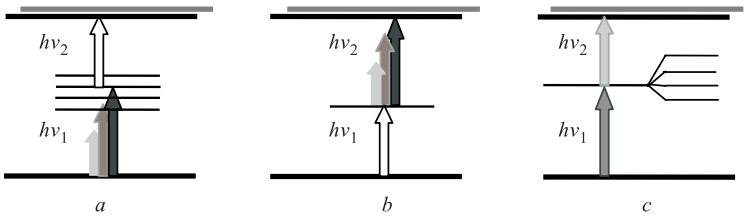

Fig. 17. Schematic representation of the atomic excitation processes of importance to the optical spectroscopy of transeinsteinium elements: *a*) search for resonance levels; *b*) determination of the IP; *c*) hyperfine spectroscopy

level schemes, both experimentally and by relativistic *ab initio* calculations, e.g., multiconfiguration Dirac–Fock (MCDF). Figure 17 illustrates the different atomic excitation processes involved in the proposed experiments. However, any atomic spectroscopy, even with the most sensitive laser methods, is hampered by the fact that a broadband search for levels is limited due to the small number of atoms available for study. To obtain reliable information under these circumstances, it is necessary to incorporate theoretical level predictions in performing the experiment.

There is an extremely pronounced mutual impact and cross fertilization between nuclear physics on one side and, laser spectroscopy and the related study of atomic properties of the super heavy elements on the other. In order to search for optical transitions and to determine the nuclear ground state properties of transuranium elements, a new facility, called SHIPTRAP, is presently being build up and tested at GSI, Darmstadt [54].

4.1. Optical Spectroscopy of Transuranium Elements. ***4.1.1. SHIPTRAP.*** SHIP (Separator for Heavy-Ion reaction Products) is a kinematical separator for reaction recoils from thin targets irradiated by beams from the heavy-ion linear accelerator UNILAC at GSI [170]. It is optimized for the separation of heavy elements produced by complete fusion of projectiles from $A = 40$ to 80 with lead or bismuth nuclei. The primary beam has an energy close to 5 MeV/u and time-averaged intensities of typically $2 \cdot 10^{12}$ to $5 \cdot 10^{12}$ ions/s.

The SHIPTRAP facility at the end of SHIP thermalizes the produced recoil ions in a noble gas from which they are then extracted and collected in a trap. The system is outlined schematically in Fig. 18. It consists of a stopping chamber containing the noble gas, an extraction system to bring the stopped ions into a vacuum region, a radiofrequency trapping system to collect the ions in this vacuum region and to cool them into well-defined bunches which are then extracted and injected into a Penning trap for isobaric purification. Thus, SHIPTRAP is an ion trap facility which is being set up to deliver very clean and cool beams of singly-

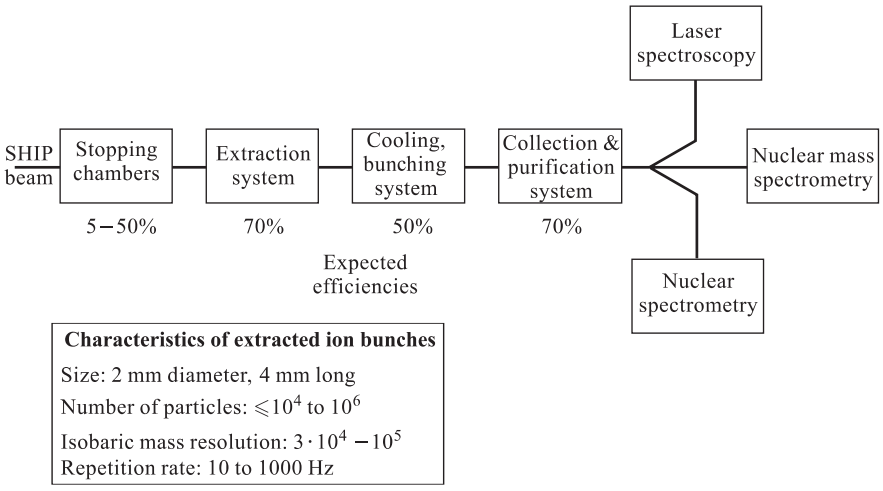

Fig. 18. Schematic view of the SHIPTRAP facility

charged recoil ions produced at the SHIP velocity filter. The small phase space and the long storage time are prerequisites for high-accuracy experiments. The purification is very important since contaminants always plagued the investigation of exotic radioactive species. This separation not only allows for very sensitive and accurate experiments to be performed within the ion trap itself but also allows the collected radionuclides to be extracted from the trap and studied in a well-defined low-emittance ion beam. Together, these possibilities open a wide range of physics applications. The physics programme of the SHIPTRAP facility comprises mass spectrometry, nuclear spectroscopy, laser spectroscopy and chemistry of transeinsteinium elements.

The present state of ion trap technology now makes it possible to couple a trap system to ion beams of higher energy (about 1 MeV/u) such as delivered by the velocity filter SHIP at GSI. A similar project has been started at a recoil separator at Argonne (USA) while at INS (Tokyo) a radiofrequency trap coupled to GARIS [171] has already been tested. The advantage of such facilities is that they enable the rich variety of physics experiments currently performed at ISOL facilities to be extended to isotopes for which target/ion source systems do not exist at ISOL facilities. The particular advantage that SHIPTRAP will have is the ability to extend these experiments to transuranic nuclides. Thus, SHIPTRAP will enable the application of refined ISOL techniques for the first time to nuclides with nuclear charge $Z > 92$, extending even to the superheavy elements of which many have a sufficiently long half-life for trap technology.

4.1.2. RADRIS Setup. The investigation of atomic and nuclear properties of transuranium elements, and especially of heavier transeinsteinium elements, for which only small samples are available requires very powerful experimental methods. The first experimental approach to this problem is a method of RAdioactive decay Detection combined with Resonance Ionization Spectroscopy in an optical buffer gas cell (RADRIS) [172]. This method combines both, very sensitive resonance ionization with pulsed lasers and low background detection of resonantly ionized species, by means of their nuclear radiation. In addition, the utilization of a high resolution α or γ spectrometer permits even the identification of a specific isotope or of an isomeric state. Advantage is taken of the facts that (i) a relative large fraction of the ions recoiling after a nuclear reaction from the target into the buffer gas neutralize, while the slowing down proceeds and (ii) the resulting atoms remain stored for about 50 ms in the laser illuminated domain before diffusing out. The latter offers the possibility for several chances to resonantly ionize the atom if a modern pulse laser system with a repetition rate greater than 100 Hz is employed. Consequently, very high resonance-ionization efficiency of the order of unity may be achieved with laser beams of mJ/cm^2 pulse energy per unit area.

The feasibility of such a scheme was firstly proved in an off-line experiment using β-active isotope ^{208}Tl ($T_{1/2} = 183$ s) [172]: the previously unknown nuclear magnetic moment $\mu(^{208}\text{Tl}) = 0.292(13)\mu_N$ and the ms radius difference between ^{208}Tl and ^{207}Tl of $\delta\langle r^2\rangle = 0.099(15)$ fm^2 have been deduced. Later, an on-line experiment with the hyperfine structure of short-lived fission isomers of americium ($Z = 95$), ^{240f}Am ($T_{1/2} = 0.9$ ms), ^{242f}Am ($T_{1/2} = 14$ ms) [173], and ^{244f}Am ($T_{1/2} = 1$ ms) [174] was carried out.

The experimental setup in its on-line modification is shown in Fig. 19. The ^{242f}Am fission isomers were produced through the $^{242}\text{Pu}(d, 2n)^{242f}\text{Am}$ reaction by pulsed deuteron beam. After post-acceleration in an electrical potential difference of 95 kV, the energy of the fission isomers was high enough to entrance the optical cell. The fission isomers rate at this place amounted typically of about 6 s^{-1}. The optical cell, filled with 30 mbar argon and 0.3 mbar nitrogen, was loaded with fission isomers in the beam-on periods. A fraction of about 13% of the recoiling ions was neutralized during the slowing process in the gas. The remaining ions are transported with an appropriate electric field onto a 250 μg/cm^2 electrode foil which was placed in front of the anticoincidence fission detector. The gas acted at the same time as a storage medium for the neutral fission isomers. The diffusion time to the cell walls was estimated to be of the order of 30 ms. Resonance ionization was performed in the beam-off periods by two colour laser beams via typical excitation scheme as shown in Fig. 20. To produce the required ionization energy of 5.97 eV, a dye laser for the first excitation step and an excimer laser for the second excitation step were used. The resonantly

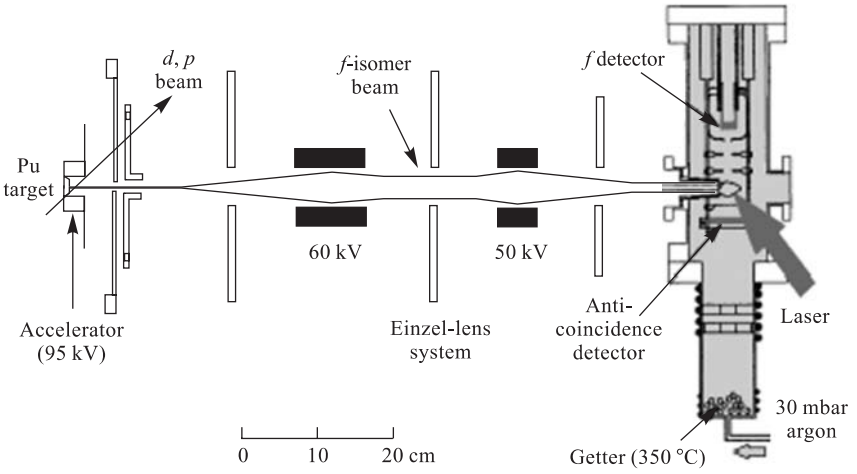

Fig. 19. Experimental setup. The fission isomers recoiling out of the target are accelerated and focused with an Einzel-lens system onto the optical buffer gas cell. The gas was purified using getter techniques to a 0.1 ppm level to avoid molecule formation of americium recoils with gas impurities (from Backe et al. [173])

ionized fission isomers were transported in the electric field of an ion electrode system to the fission detector. The average transportation time was measured to be 1.40(8) ms. A few fission events originated from isomers sticking on the foil in front of the anticoincidence detector or from neutral atoms remaining in the gas phase. However, these were completely rejected by the signal which the simultaneously emitted second fission fragments generated in the anticoincidence detector. The on-line RADRIS is sensitive enough to be applied to radioactive nuclides with short half-lives (> 1 ms) and very low production rates ($> 10\ s^{-1}$) as demonstrated with the hyperfine spectroscopy of ^{240f}Am and ^{242f}Am [173]. However, this method requires radioactive decay detection, and is not suitable for the nuclide identification if their half-lives are longer than a few minutes.

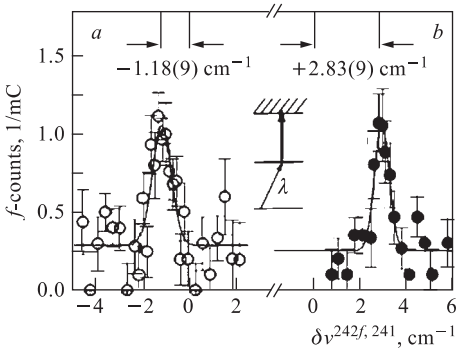

Fig. 20. Resonance ionization signals at $\lambda = 468.17$ nm (a) and $\lambda = 499.08$ nm (b) transitions. The excitation scheme is shown in the inset of b. Data acquisition time T is $T = 27$ h (a) and $T = 26$ h (b) (from Ref. 173). The IS is defined as $\delta\nu^{241,242f} = \nu^{242f} - \nu^{241}$

4.1.3. IGRIS Setup. In a further development of the resonance ionization in a buffer gas the radioactive delay detection is replaced by a mass selective direct detection of ions, as in the ion-guide quadrupole mass separation technique [175] in which the ions leaving the buffer gas cell are separated from the gas jet and mass analyzed in a quadrupole mass filter [176].

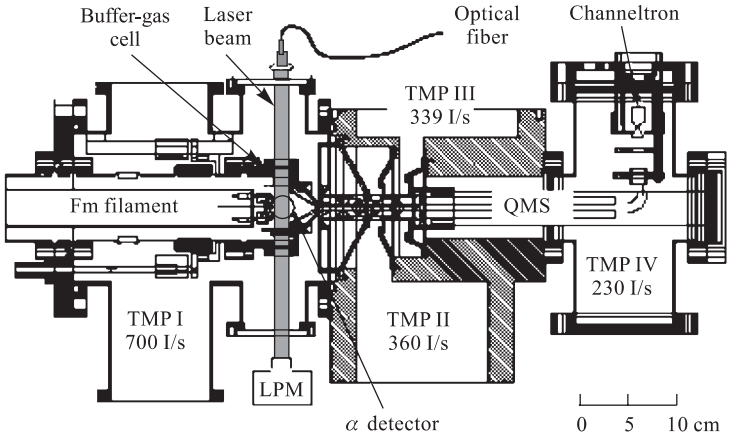

Fig. 21. IGRIS experimental setup according to [178]. The four sections are evacuated by turbomolecular pumps (TMP) with relatively low pumping speeds as indicated. QMS is the quadrupole mass spectrometer and LPM is the laser power meter. The α detectors are mounted perpendicular to the plane of drawing

A very compact apparatus (see Fig. 21) has been constructed and successfully tested at Mainz University [177, 178]. By using Ar as a buffer gas, recoils of fission reactions can be thermalized even at a low pressure. The differential pumping system consists of only one root pump and two turbo molecular pumps. Resonance ionization is performed using a two-step excitation with an excimer — dye-laser combination. The ions are transported by a suitable electric field to the nozzle, and are ejected with the ion-guide gas jet into an electrostatic lens system followed by a quadrupole mass spectrometer and a channeltron detector. To reduce the size and simplify the system, a quadrupole mass spectrometer is used instead of dipole magnet like in common ion-guide system giving the advantage, that no electrical acceleration of several kV is necessary for a high-mass resolution. This method named Ion Guide Radioactive Ionization Spectroscopy (IGRIS) provides a possibility of investigating atomic and nuclear properties of transuranium elements on line if their half lives are longer than ms. The combination of the resonance ionization spectroscopy and mass analysis provides information on both the nuclear charge number and the mass number of the ions. Moreover, the

combination of laser spectroscopy at IGRIS with SHIPTRAP facility presents a unique possibility of investigating atomic, nuclear and ion chemical properties in the region of superheavy elements.

4.2. Summary. *Nuclear Parameters — On-Line Results.* The only on-line laser experiment performed until now has been conducted by Backe et al. [173, 174] on the fission isomers of ^{240f,242f,244f}Am. It is well known that isomeric fission originates from a superdeformed nuclear shape with low excitation energy (2–3 MeV) and low spin ($I \leqslant 4$) (see, e.g., [179, 180]). Fission isomers, therefore, offer the unique possibility to test calculations of shell correction to the potential energy of the liquid nuclear drop at the state of extreme nuclear deformation. For a meaningful test a set of data as complete as possible should be available.

Table 4. **Summary of the nuclear parameters for the fission isomers ^{240f}Am, ^{242f}Am, and ^{244f}Am. The data are taken from [173, 174]**

Isomer, Af	$\Lambda^{241,Af}$, fm^2	β_2	Q, eb	$\Lambda^{Af,(A+2)f}$, fm^2	$\delta\beta_2^{Af,(A+2)f}$	$\delta Q_{20}^{Af,(A+2)f}$
240f	5.06(30)	0.690	33.9			
242f	5.34(28)	0.699	34.5	0.288(24)	0.0076(14)	0.63(8)
244f	5.41(31)	0.694	34.4	0.069(21)	−0.005	−0.1

A set of optical data for superdeformed ^{240f,242f,244f}Am has been obtained at RADRIS setup. The results are summarized in Table 4. It develops the nuclear parameter Λ^* for the fission isomers ^{240f}Am, ^{242f}Am, and ^{244f}Am relative to ^{241}Am, the quadrupole deformation parameter, β_2, and the intrinisic quadrupole moment, Q_{20}, of these isomers obtained with the deformed droplet model. The Λ values for the fission isomer pairs $[(Af, (A+2)f]$ and the changes of the deformation parameter and of the intrinisic quadrupole moment between them are given, too. The small difference of the nuclear parameter Λ between the ^{240f}Am and ^{242f}Am, and the ^{244f}Am and ^{242f}Am fission isomers results in a small change of the corresponding quadrupole moments demonstrating the stability of the superdeformation in the second potential minimum if two neutrons are removed. The experimental data is in accord with calculations of Howard and Müller [181] which predict $\delta\beta_2 = 0.00$. The experimental values of the deformation parameters are somewhat larger than the theoretically calculated $\beta_2 = 0.61$ [181] indicating that more detailed shell model calculations are required.

*Note, that for very heavy elements, $\delta\langle r^2\rangle$ in Eq. (5) must be replaced by the nuclear parameter Λ. It is an expansion into a power series of radial moments $\delta\langle r^n\rangle$ with $n \geqslant 2$ [3, 37].

Optical Data — Off-Line Measurements. The laser spectroscopic experiments on even heavier elements up to fermium ($Z = 100$) were performed off-line. At present these are atomic spectroscopy measurements corresponding to the first two steps illustrated in Fig. 17: (i) investigation of the atomic level scheme of elements with $Z > 99$, and (ii) determination of the first ionization potential of actinide elements.

(i) The ion guide-detected resonance ionization spectroscopy (IGRIS) is a very sophisticated experimental method possessing extremely high sensitivity and suitable to be applied for radioactive samples with $T_{1/2} >$ ms. This is demonstrated by the first observation of atomic levels for the heavy element fermium ($Z = 100$) reported recently by Sewtz et al. [178]. Two levels have been found by the method of two step RIS. Their wave numbers are 25099.8(2) and 25111.8(2) cm^{-1}. Partial transition rates to the $5f^{12}7s^2\ {}^3\mathrm{H}_6$ ground state have been determined from the saturation characteristics, and term assignment has been proposed. Since atomic information was not previously available for fermium, in order to predict suitable levels for a two-step resonance ionization spectroscopy, relativistic MCDF calculations have been carried out (see [178] and references therein). The agreement between experiment and calculations is striking. The results of this unique experiment give hope that the new technique will produce more spectra in this previously inaccessible corner of the periodic table.

(ii) The IP is a fundamental physical and chemical property of an element. Its accurate determination is important for identifying systematic trends in binding energy from element to element, and for drawing conclusion about the electronic structure of an atom. Reliable information about the electronic structure of the heaviest elements is needed to predict deviations from the regularities of the periodic system of elements and to help in understanding relativistic effects. Using a high accuracy Resonance Ionization Mass Spectroscopy (RIMS) the first ionization potential (IP) of Th, U, Np, and Pu were remeasured and those of Am, Cm, Bk, Cf, and Es [182, 183] were determined for the first time. The high sensitivity of RIMS enables very precise determination of the first IP of actinide elements with a sample size of $\leqslant 10^{12}$ atoms. The method RIMS is a refined powerful development of the resonance ionization spectroscopy in which additional isotope selectivity is achieved by subsequent mass analysis of the ions via a time-of-flight measurements.

Let us note once again, that the knowledge of excited atomic states of the transeinsteinium elements will allow measurements of their nuclear ground-state properties with IGRIS at SHIPTRAP. The IGRIS method is applicable if the production rates are of the order of 10 ions/s, numbers which seem to be reachable at SHIPTRAP, e.g., for the elements Md ($Z = 101$), No ($Z = 102$), and Lr ($Z = 103$) with the production cross sections in the μb range.

Collinear laser spectroscopy with fluorescence detection on a fast beam formed after SHIPTRAP system can be alternative, or even a complementary

technique, to the IGRIS method. Its resolution is better but at the expense of significant lower sensitivity. However, advantage can be taken of the pulsed character of the beam to reduce the signal background.

5. FUTURE DIRECTIONS

Clearly, our rather brief description of the laser spectroscopic methods for investigation of nuclear ground and isomeric state properties of width range of exotic nuclei and of atomic constants of transuranium elements is not complete. For example, no special attention is given to the resonance ionization spectroscopy (RIS) methods, although we mentioned their different modifications many times above. It must be noted, that since the first proposal in 1972 [184] due to the steady development and refinement of powerful pulsed as well as continuous-wave lasers, resonance ionization has developed into an extremely versatile tool for numerous applications. Apart from suppressing isobaric interferences and contributing to isotopic selectivity already in the ionization process, resonant optical excitation and ionization with laser light ensures high overall efficiency and good temporal and spatial controls of the ions delivered to mass spectrometric applications. The method first demonstrated its merits in the field of unstable nuclei, in numerous experiments at the Gatchina on-line mass separator IRIS on a series of isotopes of different rare earth-elements (see, e.g., [3] and references therein for the first publications and also [185–187] for the recent development).

The concept of a laser ion source arises in a closed connection with the RIS experiments. Instead of using ionization as a sensitive detection of optical resonance, one uses the stepwise excitation and resonance ionization process for producing ions in a hot cavity or tube. The remarkable advantages of the scheme are a very high selectivity for the particular chemical element and to some extent for a certain isotope (or isomer) as well as a good efficiency, even for elements that are difficult to ionize in conventional sources. Resonant Ionization Laser Ion Sources (RILIS) for short-lived exotic nuclei are nowadays successfully used at several places and promise to be a very important part of any second generation ISOL-based radioactive ion beam facility [188]. However, their performances — although already very useful — are not yet optimal. Substantial potential exists both on the technological side (improved laser systems) and on the physical side (new ideas to increase the selectivity and to exploit the ultimate laser band-width). Therefore, plans are underway to bring together the existing expertise in Europe on the production and use of laser-ionized exotic nuclei in order to substantially improve the performances of the laser ion source systems and thus to increase the number of beams and their quality at the presently running facilities [189]. The final result must be an improved access. This aim can be met by a further instrumentation development for the:

• Production of extremely pure ground-state and isomeric beams of exotic nuclei. These beams will open up new possibilities for experiments in the fields of nuclear-structure (ground- and isomeric-state properties, decay and reaction studies) and solid-state physics research.

• Determination of radii, spins and moments using in-source spectroscopy. This new technique, with unprecedented sensitivity, will allow extending our knowledge on radii, ground- and isomeric-state properties into the unknown territory of the nuclear chart. Since this development goes hand in hand with the production of the beams, these model-independent quantities will be determined for the most exotic nuclei.

According to Van Duppen [189] «these developments will be of interest for other fields of science (trace analysis, environmental sciences, chemistry and atomic physics) and for the future generation radioactive ion beam facilities like EURISOL, MAFF, and SPES. In order to efficiently manage the radioactivity inventory of such facilities it is essential to develop techniques that retain the major part of the nuclear reaction products in the well-confined target and ion-source region. For this the RILIS is one of the most promising methods since it allows with highest selectivity only the isotopes of the element of interest to be transmitted to the experimental setup».

CONCLUSION

This paper gives an overview of the present status of nuclear structure investigations by laser spectroscopy (the status in the field has been reviewed till August, 2003), emphasizing the successes within the past several years as well as the problems faced by the efforts to gain access to nuclear ground- and isomeric-state properties far off stability up to the drip lines. Several laser spectroscopic methods have been described. Their choice has been made according my view about the most important «blank fields» of the nuclear chart where no or only a small amount of laser spectroscopic data on nuclear structure is available. At the same time these are regions with very interesting exotic nuclear properties. Topical examples were given to stress the importance of the laser spectroscopy application in nuclear physics experiments.

Laser spectroscopy is a beautiful experimental method in nuclear physics. It studies atoms with laser light via the interaction between them. Thus, «laser spectroscopy can be used not only to study nuclear properties from the atomic spectra, but also to manipulate the atoms used for various nuclear physics experiments» [45]. Recently there has been substantial progress in our understanding of the interplay between laser spectroscopic and nuclear techniques. It is natural to expect that this fascinating connection between different methods will lead to new ideas that will drive the current efforts to experimentally realize many proposed projects.

Acknowledgements. I am very grateful to Prof. R. Neugart for the chance he gave me to participate in a part of the COLLAPS experiments on light nuclei, for valuable discussions and comments, and for giving permission for the use in this paper of recent, not yet published results on nuclear parameters of argon. Thanks are due to Prof. Yu. P. Gangrsky for the fruitful collaboration during many years and to Prof. Yu. Oganessian and Prof. Yu. E. Penionzhkevich for their continuous interest. The author is indebted to the Alexander von Humboldt Stiftung for its financial support over the years.

REFERENCES

1. *Audi G. et al.* // Nucl. Phys. A. 1997. V. 624. P. 1.
2. *Paul W.* // Rev. Mod. Phys. 1990. V. 62. P. 531.
3. *Otten E. W.* // Treatise on Heavy Ion Science. 1989. V. 8. P. 517.
4. *Gangrsky Yu. P.* // Part. Nucl. 1992. V. 23. P. 1616.
5. *Friecke G. et al.* // At. Data Nucl. Data Tables. 1995. V. 60. P. 178.
6. *Raghavan P.* // At. Data Nucl. Data Tables. 1989. V. 42. P. 189.
7. *Stone N. J.* Table of Nuclear Magnetic Dipole and Electric Quadrupole Moments. Oxford Physics (Clarendon Laboratory), 2001.
8. *Aufmuth P. et al.* // At. Data Nucl. Data Tables. 1987. V. 37. P. 455.
9. *Nadjakov E. G. et al.* // At. Data Nucl. Data Tables. 1994. V. 56. P. 133.
10. *Billowes J., Campbell P.* // J. Phys. G: Nucl. Part. Phys. 1995. V. 21. P. 707.
11. *Bergmann E. et al.* // Z. Phys. A. 1980. V. 294. P. 319.
12. *Andle A. et al.* // Phys. Rev. C. 1982. V. 26. P. 2194.
13. *Gangrsky Yu. P. et al.* // Izv. AN USSR. Ser. fiz. 1990. V. 54. P. 830.
14. *Kälber W. et al.* // Z. Phys. A. 1989. V. 334. P. 103.
15. *Tanihata I. et al.* // Phys. Rev. Lett. 1985. V. 55. P. 2676.
16. *Hansen P. G., Jensen A. S.* // Ann. Rev. Nucl. Part. Sci. 1995. V. 45. P. 591.
17. *Zhukov M. V., Thompson I. J.* // Phys. Rev. C. 1995. V. 52. P. 3505.
18. *Ozawa A. et al.* // Phys. Rev. Lett. 2000. V. 84. P. 5493.
19. *Samanta C. et al.* // Phys. Rev. C. 2002. V. 65. P. 037301.
20. *Thibault C. et al.* // Phys. Rev. C. 1975. V. 12. P. 644.
21. *Huber G. et al.* // Phys. Rev. C. 1978. V. 18. P. 2342.
22. *Guillemaud-Mueller D. et al.* // Nucl. Phys. A. 1984. V. 246. P. 37.
23. *Motobayashi T. et al.* // Phys. Lett. B. 1995. V. 346. P. 9.
24. *Touchard F. et al.* // Phys. Lett. B. 1982. V. 108. P. 169.
25. *Träger F.* // Z. Phys. A. 1981. V. 299. P. 33.
26. *Anastassov A. et al.* // Z. Phys. D. 1994. V. 30. P. 275.
27. *Gangrsky Yu. P. et al.* // J. Phys. B. 1995. V. 28. P. 957.

28. *Andersen L. H. et al.* // NuPECC Report devoted to «Impact and Applications of Nuclear Science in Europe», 2002; www.nupecc.org.
29. *Gangrsky Yu. P. et al.* // EXON-2001 / Ed. by Yu. E. Penionzhkevich, E. A. Cherepanov. Singapore, 2001. P. 523.
30. *Klein A. et al.* // Nucl. Phys. A. 1996. V. 607. P. 1.
31. *Nieminen A. et al.* // Phys. Rev. Lett. 2002. V. 82. P. 094801.
32. *Arnold E. et al.* // Phys. Lett. B. 1987. V. 197, 311.
33. *Arnold E. et al.* // Phys. Lett. B. 1992. V. 281. P. 16.
34. *Neugart R.* // Hyp. Int. 2000. V. 127. P. 101.
35. *Kalpakchieva R. et al.* // Part. Nucl. 1998. V. 29. P. 341.
36. *Bohlen H. G. et al.* // Prog. Part. Nucl. Phys. 1999. V. 42. P. 17.
37. *Kopfermann H.* Nuclear Moments. N. Y.: Academic Press, 1958.
38. *Borscher W.* PhD Thesis. University of Mainz, 1989.
39. *Vermeeren L. et al.* // Phys. Rev. A. 1990. V. 42. P. 3901.
40. *Lievens P.* // Nucl. Instr. Meth. B. 1992. V. 70. P. 532.
41. *Geithner W. et al.* Preprint CERN/INTC 2000-029; INTC/P-130.
42. *Geithner W. et al.* // Hyp. Int. 2000. V. 127. P. 117.
43. *Neugart R. et al.* // Nucl. Instr. Meth. B. 1986. V. 17. P. 354.
44. *Geithner W. et al.* Exotic Nuclei and Atomic Masses. Heidelberg, 2003. P. 88;
Geithner W. PhD Thesis. University of Mainz, 2002.
45. *Neugart R.* // Eur. Phys. J. A. 2002. V. 15. P. 35.
46. NIST — National Institute of Standards and Technology. NIST Standard Reference Database No. 78 — Atomic Spectra Database. http://physics.nist.gov/cgi-bin/AtData/main_asd. 1999.
47. *Müller A. C. et al.* // Nucl. Phys. A. 1983. V. 403. P. 234.
48. *Keim M. et al.* // Nucl. Phys. A. 1995. V. 585. P. 219.
49. *Poulsen O.* // Nucl. Instr. Meth. 1982. V. 202. P. 503.
50. *Juncar P., Pinard J.* // Rev. Sci. Instr. 1982. V. 53. P. 939.
51. *Zhao P.* // J. Opt. Soc. Am. B. 1987. V. 4. P. 644.
52. *Kugler E.* // Nucl. Instr. Meth. 1993. V. 79. P. 322.
53. *Dendooven P.* // Nucl. Instr. Meth. B. 1997. V. 126. P. 182.
54. *Dilling J. et al.* // Hyp. Int. 2000. V. 127. P. 491.
55. *Hansen P. G., Jonson B.* // Europhys. Lett. 1987. V. 4. P. 409.
56. *Riisager K.* // Rev. Mod. Phys. 1994. V. 66. P. 1105.
57. *Nörtershäuser W. et al.* // Nucl. Instr. Meth. B. 2003. V. 204. P. 644.
58. *Yan Z.-C., Drake G. W.* // Phys. Rev. A. 2000. V. 61. P. 022504.
59. *Yan Z.-C., Drake G. W.* // Phys. Rev. A. 2002. V. 66. P. 042504.
60. *Schmitt F. et al.* // Hyp. Int. 2000. V. 127. P. 111.
61. *Hanna S. S. et al.* // Phys. Rev. C. 1971. V. 3. P. 2198.
62. *Geithner W. et al.* // Phys. Rev. Lett. 1999. V. 83. P. 3792.

63. *Suzuki T. et al.* // Phys. Lett. B. 1995. V. 364. P. 69.
64. *Otsuka T. et al.* // Phys. Rev. Lett. 1993. V. 70. P. 1385.
65. *Poppelier N. A. F. M. et al.* // Z. Phys. A. 1993. V. 346. P. 11.
66. *Millener D. J., Kurath D.* // Nucl. Phys. A. 1975. V. 255. P. 315.
67. *Millener D. J. et al.* // Phys. Rev. C. 1983. V. 28. P. 497.
68. *Fortier S. et al.* // Phys. Lett. B. 1999. V. 461. P. 22.
69. *Aumann T. et al.* // Phys. Rev. Lett. 2000. V. 84. P. 35.
70. *Ozawa A. et al.* // Phys. Lett. B. 1994. V. 334. P. 18.
71. *Guimaraes V. et al.* // Nucl. Phys. A. 1995. V. 588. P. 161c.
72. *Nakamura S. et al.* // Phys. Lett. B. 1998. V. 416. P. 1.
73. *Baby L. T. et al.* // J. Phys. G: Nucl. Part. Phys. 2004. V. 30. P. 519.
74. *Ueno H. et al.* // Phys. Rev. C. 1996. V. 53. P. 2142.
75. *Sugimoto K.* // J. Phys. Soc. Japan (Suppl.). 1973. V. 34. P. 197.
76. *Warburton E. K., Brown B. A.* // Phys. Rev. C. 1992. V. 46. P. 923.
77. *Fortune H. T., Sherr R.* // Phys. Lett. B. 2001. V. 503. P. 70.
78. *Timofeyuk N. K. et al.* // Nucl. Phys. A. 1996. V. 600. P. 1.
79. *Warner R. E. et al.* // Nucl. Phys. A. 1998. V. 635. P. 292.
80. *Poves A., Retamosa J.* // Nucl. Phys. A. 1994. V. 571. P. 221.
81. *Caurier E. et al.* // Phys. Rev. C. 1998. V. 58. P. 2033.
82. *Pritychenko B. V. et al.* // Phys. Lett. B. 1999. V. 461. P. 322.
83. *Touchard F. et al.* // Phys. Rev. C. 1982. V. 25. P. 2756.
84. *Keim M. et al.* // Hyp. Int. 1995. V. 97/98. P. 543; Eur. Phys. J. A. 2000. V. 8. P. 31.
85. *Geithner W. et al.* // Hyp. Int. 2000. V. 129. P. 271.
86. *Carchidi M. et al.* // Phys. Rev. C. 1986. V. 34. P. 2280.
87. *Preedom B. M., Wildenthal B. H.* // Phys. Rev. C. 1972. V. 6. P. 1633.
88. *Gangrsky Yu. P. et al.* // Eur. Phys. J. A. 1998. V. 3. P. 313.
89. *Yei W. et al.* // Phys. Rev. A. 1993. V. 48. P. 1909.
90. *Jönsson P. et al.* // Phys. Rev. A. 1996. V. 53. P. 4021.
91. *Campi X. et al.* // Nucl. Phys. A. 1975. V. 251. P. 193.
92. *Bohr A., Mottelson B.* Nuclear Structure (Nuclear Deformation). Singapore; New Jersey; London; Hong-Kong: World Scientific, reprint 1998 ed. V. 2.
93. *Goriely S. et al.* // At. Data Nucl. Data Tables. 2001. V. 77. P. 311.
94. *Raman S. et al.* // Ibid. V. 78. P. 1.
95. *Siiskonen T. et al.* // Phys. Rev. C. 1999. V. 60. P. 034312.
96. *Kitagawa H. et al.* // Z. Phys. A. 1997. V. 358. P. 381;
Reinhard P. G. Private Communication. 2001.
97. *Meyrs W. D., Schmidt K.-H.* // Nucl. Phys. A. 1983. V. 410. P. 61.
98. *Möller P. et al.* // At. Data Nucl. Data Tables. 1995. V. 59. P. 185.

99. *Lalazisis G. A. et al.* // Nucl. Phys. A. 1998. V. 628. P. 221.
100. *Lalazisis G. A. et al.* // At. Data Nucl. Data Tables. 1999. V. 71. P. 1.
101. *Rodríguez-Guzmán R. R. et al.* // Eur. Phys. J. A. 2003. V. 17. P. 37.
102. *Brown B. A., Wildenthal B. H.* // Nucl. Phys. A. 1987. V. 474. P. 27.
103. *Warburton E. K. et al.* // Phys. Rev. C. 1990. V. 41. P. 1147.
104. *Geithner W. et al. (COLLAPS (Mainz)–ISOLDE (CERN) Collab.).* Nuclear Moments and Charge Radii of Argon Isotopes Between Neutron Shell Closures $N = 20$ and $N = 28$. To be published.
105. *Balabansky D. et al.* CERN INTC-2003-012; INTC-I-045. 2003.
106. *Savard G.* // Nucl. Phys. A. 2001. V. 701. P. 292.
107. *Barranco F., Broglia R. A.* // Phys. Lett. B. 1985. V. 151. P. 90.
108. *Caurier E. et al.* // Phys. Lett. B. 2001. V. 522. P. 240.
109. *Äystö J. et al.* Proposal for SHIPTRAP: www-aix.gsi.de/∼shiptrap/proposal.pdf. 1998.
110. *Nieminen A. et al.* // Nucl. Instr. Meth. A. 2001. V. 469. P. 244.
111. *Billowes J.* // Nucl. Phys. A. 2001. V. 682. P. 206c.
112. *Levins J. M. G. et al.* // Phys. Rev. Lett. 1999. V. 82. P. 2476.
113. *Forest D. H. et al.* // J. Phys. G: Nucl. Part. Phys. 2002. V. 28. P. L63.
114. *Campbell P. et al.* // Eur. Phys. J. A. 2002. V. 15. P. 45.
115. *Campbell P. et al.* // Phys. Rev. Lett. 2002. V. 89. P. 082501.
116. *Gangrsky Yu. P. et al.* // JINR Rapid Commun. 1995. No. 1[69]. P. 5.
117. *Buck B. et al.* // Phys. Rev. C. 1995. V. 52. P. 1840.
118. *O'Leary C. D. et al.* // Phys. Rev. C. 2000. V. 61. P. 064314.
119. *Krasta T. et al.* // Rus. J. Nucl. Phys. 2002. V. 65. P. 752.
120. *Nguyen Van Giai, Sagawa H.* // Nucl. Phys. A. 1981. V. 371. P. 1; Phys. Lett. B. 1981. V. 106. P. 379.
121. *Retamosa J. et al.* // Phys. Rev. C. 1997. V. 55. P. 1266.
122. *Ring P., Schuck P.* The Nuclear Many-Body Problem. Berlin: Springer Verlag, 2000.
123. *Vermeeren L. et al.* // Phys. Rev. Lett. 1992. V. 68. P. 1679.
124. *Sharma M. M. et al.* // Phys. Lett. B. 1993. V. 317. P. 9.
125. *Lalasisis G. A., Sharma M. M.* // Nucl. Phys. A. 1995. V. 586. P. 201.
126. *Zamick L.* // Ann. Phys. 1971. V. 66. P. 784.
127. *Talmi I., Unna I.* // Ann. Rev. Nucl. Sci. 1960. V. 10. P. 353.
128. *Wohlfahrt H. H. et al.* // Phys. Rev. C. 1981. V. 23. P. 533.
129. *Talmi I.* // Nucl. Phys. A. 1984. V. 423. P. 189.
130. *Werner T. R. et al.* // Nucl. Phys. A. 1996. V. 597. P. 327.
131. *Gangrsky Yu. P. et al.* Charge Radii and Nuclear Moments of Sc Isomers by Laser Spectroscopy. Proposal 182. JYFL Accelerator Laboratory, 2003.
132. *Aboussir Y. et al.* // Nucl. Phys. A. 1992. V. 549. P. 155.
133. *Le Blanc F. et al.* // Phys. Rev. C. 1999. V. 60. P. 054310.
134. *Kluge H.-J., Nörterhäuser W.* GSI Preprint 2003-02.

135. *Buchinger F. et al.* // Phys. Rev. C. 1990. V. 41. P. 2883.
136. *Raman S. et al.* // At. Data Nucl. Data Tables. 1987. V. 36. P. 1.
137. *Möller P., Nix J. R.* // At. Data Nucl. Data Tables. 1981. V. 59. P. 185.
138. *Thayer H. L. et al.* // J. Phys. G: Nucl. Part. Phys. 2003. V. 29. P. 2247.
139. *Kugler E.* // Hyp. Int. 2000. V. 129. P. 23.
140. *Nakamura T. et al.* // Opt. Commun. 2002. V. 205. P. 329.
141. *Äystö J.* // Nucl. Phys. A. 2001. V. 693. P. 477.
142. *Oganessian Yu. Ts., Zagrebaev V. I.* Project DRIBs. 1999; http//flerovlab.jinr.ru/flnr/index.html/
143. *Dombsky M. et al.* // Nucl. Phys. A. 2002. V. 702. P. 486c.
144. *Polikanov C. M.* // JETP. 1962. V. 42. P. 1465.
145. *Nolan P. J., Twin P. J.* // Ann. Nucl. Part. Sci. 1998. V. 38. P. 533.
146. *Janssens P. V., Khoo T. L.* // Ann. Rev. Nucl. Part. Sci. 1991. V. 41. P. 321.
147. *Bohr A., Weisskopf V. F.* // Phys. Rev. 1950. V. 77. P. 94.
148. *Pyyko P.* // Mol. Phys. 2001. V. 99. P. 1617.
149. *Berkes I. et al.* // Hyp. Int. 1992. V. 75. P. 93.
150. *Lhersonneau G. et al.* // Phys. Rev. C. 1994. V. 49. P. 1379.
151. *Urban W. et al.* // Nucl. Phys. A. 2001. V. 689. P. 605.
152. *Mach H.* // Nucl. Phys. A. 1991. V. 523. P. 197.
153. *Ragnarsson I.* // Phys. Scripta. 1984. V. 29. P. 385.
154. *Sauvage J. et al.* // Hyp. Int. 2000. V. 127. P. 303.
155. *Lettry J. et al.* // Rev. Sci. Instr. 1998. V. 69. P. 761.
156. *Neugart R.* // Instr. Phys. Conf. Ser. 1992. V. 132. P. 133.
157. *Le Blanc F. et al.* // Eur. Phys. J. A. 2002. V. 15. P. 49.
158. *Vautherin D., Brink D. M.* // Phys. Rev. C. 1972. V. 5. P. 626.
159. *Dechargé J., Gogny D.* // Phys. Rev. C. 1980. V. 21. P. 1568.
160. *Girod M., Grammaticos B.* // Phys. Rev. C. 1983. V. 27. P. 2317.
161. *Girod M. et al.* // Phys. Rev. Lett. 1989. V. 62. P. 2452.
162. *Quentin P. et al.* // Rev. Nucl. Sci. 1978. V. 28. P. 523.
163. *Patyk Z. et al.* // Phys. Rev. C. 1999. V. 59. P. 704.
164. *Reinhard P. G.* // Rep. Prog. Phys. 1989. V. 52. P. 439.
165. *Anselment M. et al.* // Nucl. Phys. A. 1986. V. 451. P. 471.
166. *Piller C. et al.* // Phys. Rev. C. 1990. V. 42. P. 182.
167. *Wapstra A. H., Audi G.* // Eur. Phys. J. A. 2002. V. 15. P. 1.
168. *Cheal B. et al.* // J. Phys. G: Nucl. Part. Phys. 2003. V. 29. P. 2479.
169. *Hofmann S., Münzenberg G.* // Rev. Mod. Phys. 2000. V. 72. P. 733.
170. *Miinzenberg G. et al.* // Nucl. Instr. Meth. 1979. V. 161. P. 65.
171. *Fujitaka S. et al.* // Nucl. Instr. Meth. B. 1997. V. 126. P. 386.
172. *Lauth W. et al.* // Phys. Rev. Lett. 1992. V. 68. P. 1675.

173. *Backe H. et al.* // Phys. Rev. Lett. 1998. V. 80. P. 920.
174. *Backe H. et al.* // Hyp. Int. 2000. V. 127. P. 35.
175. *Iivonen A. et al.* // Phys. Scr. 1990. V. 42. P. 133.
176. *Ärje J. et al.* // Nucl. Instr. Meth. B. 1987. V. 26. P. 384.
177. *Backe H. et al.* // Nucl. Instr. Meth. B. 1997. V. 126. P. 406.
178. *Sewtz M. et al.* // Phys. Rev. Lett. 2003. V. 90. P. 163002.
179. *Metag V. et al.* // Phys. Rep. 1980. V. 65. P. 1.
180. *Bjornholm S., Lynn J. E.* // Rev. Mod. Phys. 1980. V. 52. P. 727.
181. *Howard W. M., Möller P.* // At. Data Nucl. Data Tables. 1980. V. 25. P. 219.
182. *Erdmann N. et al.* // J. Alloys Compounds. 1998. V. 271/273. P. 837.
183. *Peterson J. R. et al.* // Ibid. P. 876.
184. *Ambartsumian R. V., Letokhov V. S.* // Appl. Opt. 1972. V. 11. P. 354.
185. *Alkhazov G. D. et al.* // Nucl. Instr. Meth. B. 1992. V. 69. P. 517.
186. *Barzakh A. E. et al.* // INPC 2001 Berkeley. AIP Conf. Proc. V. 610. P. 915.
187. *Panteleev V. N. et al.* // Rev. Sci. Instr. 2002. V. 73. P. 738.
188. *Fedosseev V. N. et al.* // Nucl. Instr. Meth. B. 2003. V. 204. P. 353.
189. *Van Duppen P.* Laser Techniques for Exotic Nuclei Research. 2002. P. 35; http://www.finuphy.org/doc/.